INSTITUTO SUPERIOR DE ENGENHARIA DO PORTO
MESTRADO EM ENGENHARIA MECÂNICA




Strength and damage analysis of composite-aluminium adhesively-bonded single-lap joints

TIAGO EMANUEL ANDRADE RIBEIRO
Outubro de 2015

POLITÉCNICO
DO PORTO

Strength and damage analysis of composite-aluminium adhesively-bonded single-lap joints

Tiago Emanuel Andrade Ribeiro

A thesis submitted in conformity with the requirements for the Master Degree in

Mechanical Engineering

Instituto Superior de Engenharia do Porto

Departamento de Engenharia Mecânica

06 October 2015

Report of the discipline of Dissertation/Project/Internship of the 2nd year of the Master Degree in Mechanical Engineering

Candidate: Tiago Emanuel Andrade Ribeiro, 1081605@isep.ipp.pt

Supervisor: Raul Duarte Salgueiral Gomes Campilho, RDS@isep.ipp.pt

Co-Supervisor: Luca Goglio, luca.goglio@polito.it

Co-Supervisor: Mariana Doina Banea, mdbanea@gmail.com

Co-Supervisor: Lucas Filipe Martins da Silva, lucas@fe.up.pt

Mestrado em Engenharia Mecânica
Departamento de Engenharia Mecânica

Instituto Superior de Engenharia do Porto

06 October 2015

A todos que me acompanharam durante os últimos dois anos

Acknowledgements

For all the love, guidance and support in all decisions during my life and in particular during this thesis, in first place, I want to express my gratitude to my parents Armando Augusto da Costa Ribeiro and Maria José Martins Andrade Ribeiro.

I want to express my sincere acknowledgement to my brother Jorge Gabriel Andrade Soares Ribeiro and his wife Helena Maria Moreira Ferreira Soares Ribeiro for all the support and interest in my academic career and in this thesis. I also want to thank their children Nuno Miguel Soares Ribeiro and Rui Pedro Soares Ribeiro for all the funny moments that were important to get apart of all the pressure during the work of this thesis. I cannot forget my godmother Carla Sofia Loureiro and family for all the interest and support.

Special acknowledgements to my supervisor, Dr. Raul Duarte Salgueiral Gomes Campilho, Senior Lecturer at Instituto Superior de Engenharia do Porto for the invaluable support in making this thesis in Italy, for his expertise, intelligence, dexterity and large experience in handling the most complex and multidisciplinary problems, for his counselling and help.

My Acknowledgement to Dr. Luca Goglio, Senior Lecturer at Politecnico di Torino and co-supervisor of this dissertation, for the support and help during my first days at Torino and all the technical advices, expertise and help during the execution of this Thesis.

Thanks to Dr. Ricardo Carbas and Dr. Mariana Banea, researchers at Faculdade de Engenharia da Universidade do Porto and specialists in adhesive joints for all the help, advice, availability and information provided during the experimental tests of this thesis. I also want to thank Dr. Lucas Filipe Martins da Silva for providing the facilities to develop the experimental part of the work.

Acknowledgements to the Instituto Superior de Engenharia do Porto, Politecnico di Torino, Faculdade de Engenharia da Universidade do Porto and Erasmus Program for this magnificent opportunity, which broadened my horizons.

Special and sincere thanks for my long-standing friend Nuno Santos and his wife Cátia Teixeira for all the friendship, conversations, support and advices not only during this thesis but also during all these years that have passed.

I want to thank to all my friends for staying after all these years and direct or indirectly leave a mark in this thesis, Nuno Domingues, Sofia Alves, Tiago Fernandes and Pedro Santos.

I express my sincere acknowledgement to Manuel Fernando Moutinho Mendes for giving unconditional support and good working conditions that I had at his company (Mendos Lda), he was preponderant to the success in this thesis and in this master degree. Special thanks to my co-workers Bruno Barbosa, Gil Vieira and Firmino Torres, which are part of this success.

Thanks to Tiago Bompastor and Nuno Veiga for all the help during this master degree and, in particularly, to Rui Araújo for all the guidance, expertise and working methods that were important during the last two years and that I will apply in the future.

Last but not least, I also want to thank Ignacio Rojas, Nico Zaccarelli, João Oliveira and Pietro La Torre for all the good moments that we spent in Italy.

Abstract

With the need to find an alternative way to mechanical and welding joints, and at the same time to overcome some limitations linked to these traditional techniques, adhesive bonds can be used. Adhesive bonding is a permanent joining process that uses an adhesive to bond the components of a structure. Composite materials reinforced with fibres are becoming increasingly popular in many applications as a result of a number of competitive advantages. In the manufacture of composite structures, although the fabrication techniques reduce to the minimum by means of advanced manufacturing techniques, the use of connections is still required due to the typical size limitations and design, technological and logistical aspects. Moreover, it is known that in many high performance structures, unions between composite materials with other light metals such as aluminium are required, for purposes of structural optimization.

This work deals with the experimental and numerical study of single lap joints (SLJ), bonded with a brittle (Nagase Chemtex Denatite XNRH6823) and a ductile adhesive (Nagase Chemtex Denatite XNR6852). These are applied to hybrid joints between aluminium (AL6082-T651) and carbon fibre reinforced plastic (CFRP; Texipreg HS 160 RM) adherends in joints with different overlap lengths (L_O) under a tensile loading. The Finite Element (FE) Method is used to perform detailed stress and damage analyses allowing to explain the joints' behaviour and the use of cohesive zone models (CZM) enables predicting the joint strength and creating a simple and rapid design methodology. The use of numerical methods to simulate the behaviour of the joints can lead to savings of time and resources by optimizing the geometry and material parameters of the joints. The joints' strength and failure modes were highly dependent on the adhesive, and this behaviour was successfully modelled numerically. Using a brittle adhesive resulted in a negligible maximum load (P_m) improvement with L_O. The joints bonded with the ductile adhesive showed a nearly linear improvement of P_m with L_O.

Keywords

Hybrid joints, Single-lap joint, Cohesive zone models, Stress distributions, Damage analysis.

Resumo

Com a necessidade de encontrar formas alternativas às juntas mecânicas e soldadas que permitisse ligar componentes de forma mais vantajosa, surgiram as juntas adesivas. Estas caracterizam-se por ser um processo permanente onde é usado um adesivo para unir componentes de uma estrutura que não poderiam ser construídas numa peça só. Materiais compósitos reforçados com fibras estão a ser cada vez mais utilizados nas mais variadas aplicações devido às suas propriedades mecânicas vantajosas quando comparados com os materiais tradicionais de engenharia. Na construção de estruturas em materiais compósitos o uso de ligações continua a ser necessário devido a limitações dimensionais, tecnológicas e logísticas. Para além disso, é necessária a combinação de materiais compósitos com ligas de alumínio para otimização estrutural.

Este trabalho refere-se ao estudo de juntas de sobreposição simples ligadas com dois tipos de adesivos, um adesivo considerado frágil (Nagase Chemtex Denatite XNRH6823) e um considerado dúctil (Nagase Chemtex Denatite XNR6852). Estes foram aplicados em juntas híbridas entre uma liga de alumínio (AL6082-T651) e um material compósito reforçado com fibra de carbono (Texipreg HS 160 RM) em juntas com diferentes valores de sobreposição sendo sujeitos a um ensaio de tração. Foi efetuada uma análise experimental, cujos resultados foram comparados posteriormente com uma análise numérica. O Método de Elementos Finitos foi usado para realizar uma análise de tensões e dano, e a resistência das juntas foi prevista por Modelos de Dano Coesivo. O uso de modelos numéricos permite a redução de tempos de projeto e otimização da estrutura. O comportamento das juntas foi corretamente modelado numericamente e concluiu-se que a resistência da junta e modos de rotura dependem do tipo de adesivo. A aproximação numérica demonstrou ser bastante precisa, sendo que o adesivo frágil teve resultados mais aproximados da realidade quando comparados com os resultados do adesivo dúctil.

Palavras-chave

Juntas híbridas, Juntas de sobreposição simples, Modelos de dano coesivo, Distribuição de tensões, Análise de dano.

Index

Figures Index

Tables Index

Nomenclature

Roman characters

b – Specimen width

E – Young's modulus

G – Shear modulus, strain energy release rate

G_C – Fracture toughness

G_{IC} – Normal mode fracture energy

G_{IIC} – Shear mode fracture energy

G_{IIIC} – Tear mode fracture energy

$\mathbf{K_{COH}}$ – Stiffness matrix

k_{nn}, k_{ss}, k_{ns} – Stiffness parameters

L_O – Overlap length

L_S – Adherend length

L_T – length between shims

P – Load

P1, P2, P3, P4, P5 – Horizontal planes for the stress distributions

P_m – Maximum load

t – Stress vector

t_A – Adhesive thickness

t_m^0 – Mixed-mode cohesive strength

t_n – Current shear cohesive strength

t_n^0 – Tensile cohesive strength

t_S – Adherend thickness

t_s – Current tensile cohesive strength

t_s^0 – Shear cohesive strength

x – Distance from the free overlap edge

$\boldsymbol{\delta}$ – Displacement vector

Greek characters

α, β and γ – Power law parameters in mixed-mode criteria

δ – displacement

δ_m^0 – Mixed-mode displacement corresponding to t_m^0

δ_m^f – Mixed mode failure displacement

δ_n – Tensile displacement

δ_n^0 – Tensile displacement corresponding to t_n^0

δ_n^f – Tensile failure displacement

δP_m – Displacement corresponding to the maximum load

δ_s – Shear displacement

δ_s^0 – Shear displacement corresponding to t_s^0

δ_s^f – Shear failure displacement

$\boldsymbol{\varepsilon}$ – Strain vector

ε – strength

ν – Poisson's ratio

σ_y – Through thickness normal stresses, yield strength

τ_{avg} – Average shear stress

τ_{xy} – Shear stress

Abbreviations

2D – Two dimensions

3D – Three dimensions

ASTM – American Society for Testing and Materials

CFRP – Carbon fibre reinforced plastic

CZM – Cohesive zone model

FE – Finite element

SDEG – Stiffness degradation

SLJ – Single-lap joints

1 Introduction

1.1 Framework

With the recent development of vehicles and the need of reducing their weight in order to achieve the best performance and, at the same time, reduce the energy consumption, composite materials with polymeric matrix are being increasingly used. This is because of their good mechanical, chemical and physical properties. Joining methods between these materials and aluminium are also being increasingly used in the aerospace, aeronautical and automotive industries, enabled by the quick technological evolution of manufacturing process. This type of joining, when compared to the traditional mechanical joints, has showed several advantages, such as better stress distributions, smaller weight, increased fatigue strength and good strength/weight ratio.

Taking the next generation airbus A350 XWB as an example, more than 50% of the structure is made of composites [1]. In the automotive industry, for example, Alfa Romeo and BMW used composite materials in body panels and chassis in the model 4C and I8, respectively [2, 3]. With the increasing use of adhesive bonds in structural applications, it is important to know how to predict their strength using numerical methods. Actually the existence of quick and accurate design tools can have a direct impact in the industry in order to reduce costs, design time and optimize the structure before the development of the first prototypes.

1.2 Objectives

This project aims at investigating the behaviour of single-lap joints (SLJ) with different values of overlap length (L_O) using adhesive bonds between carbon fibre reinforced plastic

(CFRP) and aluminium alloy adherends with two adhesives of distinct ductility, the brittle (XNRH6823) and the ductile (XNR6852).

The first stage consists of manufacturing the SLJ in the laboratory, test them and analyse the failure modes. Afterwards a Finite Elements (FE) program to perform a detailed analysis of the different type of joints with the objective of comparing the numerical results with the experimental will be used. In the end, it is expected that a simple but robust design tool is made available for this type of joints.

1.3 Calendar

The work developed in this thesis followed the timetable depicted in Table 1.

Table 1 – Timetable of the current thesis

	2014						2015					
	March	April	May	Jun to Sept	October	November	December	January	February	March	April	May to Sept
Bibliographic work	■	■	■		■	■	■		■	■		
Experimental work	■	■	■									
Numerical work					■	■	■					
Thesis writing									■	■	■	■

1.4 Thesis layout

This thesis is structured as follows

In Section 1 an introduction of the subject and the objectives of this study are presented.

Section 2 presents the bibliographic revision that discusses the state-of-the-art, relevant information regarding bonded joints. Typical loads and failures are explained, as well the most relevant techniques for strength prediction of bonded and hybrid joints are presented.

In Section 3, all the experimental work is described and the tests results are presented and discussed. First, the characteristics of the materials used to manufacture the joints are presented. Next, the manufacturing process of the two types of adherends and respective surface treatments in order to improve the adhesive adhesion are detailed, followed by the joint fabrication and the techniques that were used to guarantee the standardization of the different joints. Finally, the experimental results are presented.

Section 4 is related to the numerical analysis. Initially, all the parameters and numeric conditions used in the FE analysis (by Cohesive Zone Models; CZM) are described. A peel and shear stress analysis in the elastic stage of load is afterwards conducted at several horizontal planes in the joints and between different values of L_O. Following, a damage analysis of the CZM elements throughout the bond is then carried out at two different planes (CFRP and adhesive layer) for a better perception of the gradual failure process. Finally, the results of the numerical analysis are compared to the experimental results and the differences between joint configurations (adhesive type and value of L_O) discussed based on the previous stress and damage analyses.

In the last Section, all the conclusions of the work are summarized and suggestions for future works are presented.

2 Bibliographic work

2.1 Adhesive bonding of components

From the early years of industry, the need to join different materials and structures was always present. Mechanical joints are a well-proved joining method and the most common due to its simplicity, quickness and the possibility of being reverted. Welding is used mainly in the union of metallic materials, and suitable to apply in structures that do not need to be disassembled. Currently, adhesive bonds are increasingly being subject of study and development. Comparatively with mechanical joints, adhesive bonds have the advantage of better stress distributions, lower weight, absorbing dynamic loadings, sealing capabilities and efficient joining of thin sheets. Adhesives can also join two different materials without contacting between them, and thereby preventing chemical reactions [4].

This type of joints is very specific and not as easy to manufacture as, for example, mechanical joints. Some procedures have to be undertaken before bonding, and specific equipment is required. Also, it is necessary to clean the surfaces to be joined and, in some cases, mechanical and chemical treatment is required to ensure good adherence. Then, the adhesive has to be chosen based on the properties of the adherends and on the application. The development and design of the joint cannot be overlooked, since it is important to ensure that the failure is cohesive in the adhesive layer in order to maximise the joint strength. Another important issued to consider is the fabrication time. Some adhesives have a long curing time and sometimes autoclave is necessary to ensure the best possible physical properties are repeatedly attainable.

2.1.1 Bonded joints characterization

Adhesive bonded joints are an alternative to traditional joining techniques, which uses adhesives to join two adherends. The adhesive is a polymeric material that, when applied to the surfaces of the adherends, can join them together and resist separation. Adhesives that can resist more than 6.7 MPa are called structural adhesives [5].

There are a lot of advantages that are responsible for the increasing usage of adhesive joints, such as [6]:

- Possibility to join dissimilar materials;
- Absence of contact between the parts to be joined, which could otherwise lead to galvanic corrosion;
- Good noise and vibration damping properties;
- High mechanical strength and joint sealing capabilities;
- Lower stress concentrations because the load is more evenly distributed;
- Cost-effective technique if automatized.

However, adhesives joints have some limitations that have to be considered before choosing this technique.

- The surface pre-treatment of the adherends has a major effect on the strength of the joint;
- Limited service temperature when compared with classical techniques;
- Adhesive joints are week in peel, and the project designer should select a joint configuration that minimizes peel stresses;
- Some adhesives need high temperatures to cure;
- Some adhesives require curing in an autoclave, which reflects other fabrication costs.

2.1.2 Common applications of bonded joints

The use of adhesively bonded joints is present in several areas. This advantages, when compared to the traditional joints, make them appropriated in many industries like wind energy, marine, transportation, automotive and construction.

In the wind energy industry the low weight, fatigue resistance and absence of aerodynamic disturbance are important requirements. The wind turbine blade is an aerodynamic structure which consists of skin and webs. Adhesive joining is used to assemble the parts of the blade, as shown in Figure 1. In this specific application, adhesive joints have fewer sources of stress concentrations, higher toughness and more uniform stresses distributions through the joined area compared with mechanically fastened joints, such as rivets and screws. In large scale turbine blades, adhesive bond lines are thick and much longer than in other applications, and the web to skin bond line spans along the entire length of the blade [7].

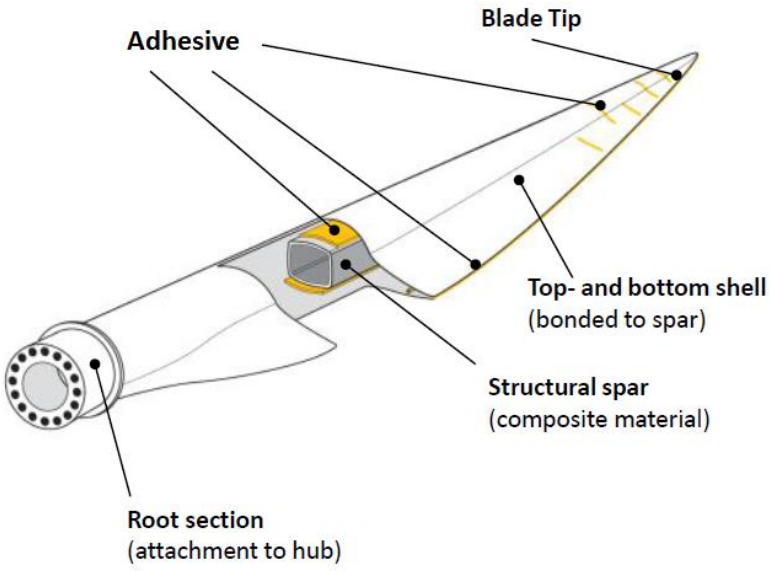

Figure 1 – Adhesive bonding applied to wind blades [8]

In the shipyards industry, adhesives and sealants are used in many applications: to bond the hull/deck, the channels running through the teak-made deck staves, the sea chests, the exhaust systems, the air intakes, the portholes, the windshields and the cabin panels inside the boat. Different types of commercial adhesives are represented in Figure 2 [9]. Due to the aggressive environmental conditions, adhesives started to be used in related applications when their resistance to deterioration, temperature and humidity permitted a stable behaviour under these conditions.

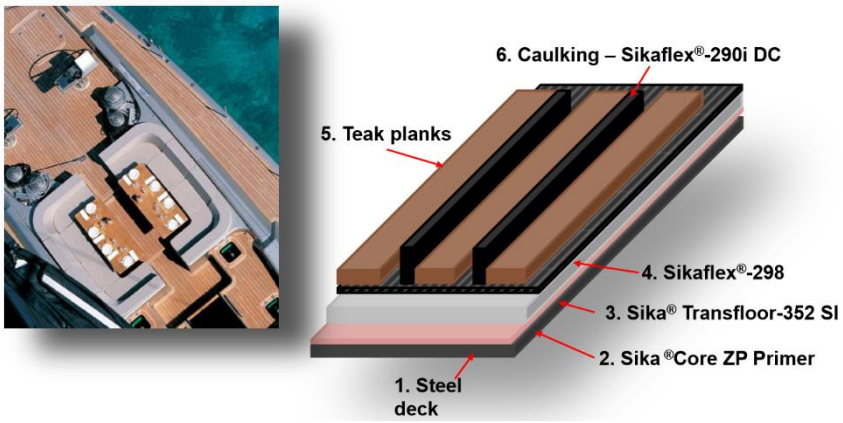

Figure 2 – Adhesive bonding in the shipyard industry [8]

In the past years, road transports became heavier due to safety regulations and increasing of technology applied in the transportation, leading to an increase of the fuel consumption. Thus, reducing the weight is nowadays a preponderant goal in automotive industry. To solve this problem, different materials have been used in several parts in order to maximize the stiffness while reducing the weight. To join this different materials, the automotive industry started to implement what the aerospace industry has been using for decades, namely adhesives for joining load-bearing components.

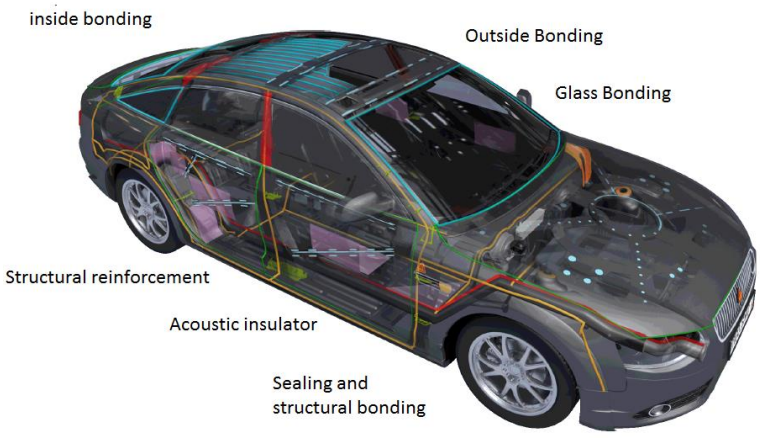

Figure 3 – Adhesive bonding in the automotive industry [8]

The main method of joining steel sheets in the automotive industry has been spot-welding, but this method requires access to both sides of the joint, it cannot join aluminium effectively, or composites at all, and it generally destroys any coatings used to improve the corrosion resistance of steels. These disadvantages of spot-welds can be solved using adhesive bonding. High-strength adhesives are used where the adhesive is supposed to play

a primary role in the joining and strength of a structure. Generally, toughened, single-part paste epoxies are used for structural bonding of car body shells [10]. Other applications of adhesives in the automotive industry include acoustic insulation and sealing, as it can be seen in Figure 3.

2.1.3 Typical loads

Adhesive joints are typically three-dimensional structures, therefore a bonded joint usually is subjected to several loads like tensile, shear, cleavage, peel and compression (Figure 4). It is very important to minimize peel loads to the minimum and to understand how the joint will behave.

The main loads are shear and peel but a brief explanation of the different type of loads will be given.

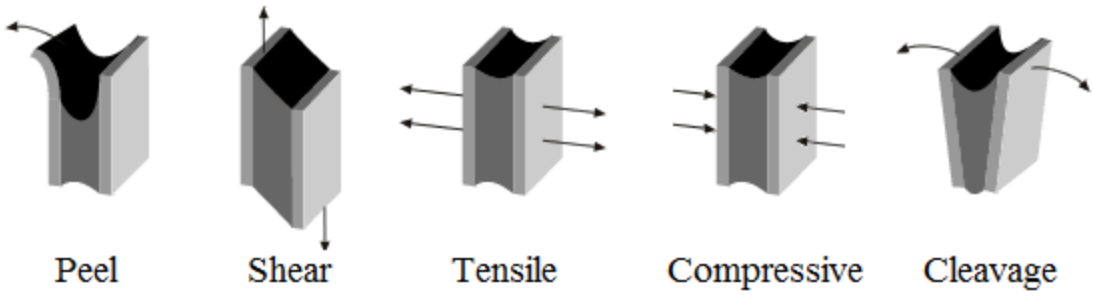

Figure 4 – Loads in a bonded joint [11]

Peel stresses are common in bonded joints. With the increase of the applied load, the specimens tend to bend, (especially with non-collinear adherends) this leads to peel stresses that occur due to the asymmetry and elastic deformation of the joint. These stresses highly reduce the joints' strength since they usually concentrate at very restricted regions and, as said before, it is extremely important to minimize these loads. A schematic representation of the phenomenon leading to peel stresses is presented in Figure 5 since the loads are not collinear, a section of the adherend tends to overturn due to the bonding moment created by the load offset. This overturning moment must be reacted by either peel stresses present within the adhesive layer, or by a resisting moment within the adherend. Either of these involves an out-of-plane deformation of the adherend and the associated peel stresses [11].

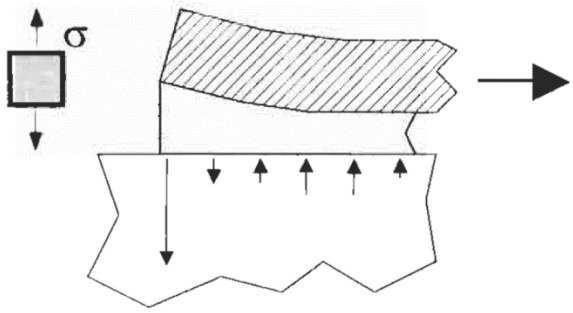

Figure 5 – Development of peel stresses in an adhesive joint [11]

The shear lag model [11] is one of the most fundamental concepts in the transfer of load by shear between two members joined by an adhesive. When a joint is axially loaded, the shear stress is distributed according to the stiffness of the adhesive along the length of the bond, as shown in Figure 6. Shear stress distributions depend on the type of the adherends. If the adherends are rigid, the distribution is more uniform, with the load being gradually transferred across the bond length with small stress gradients. If the adherends are more compliant, significant stress will occur at the end of the joints, as shown in Figure 7 [11].

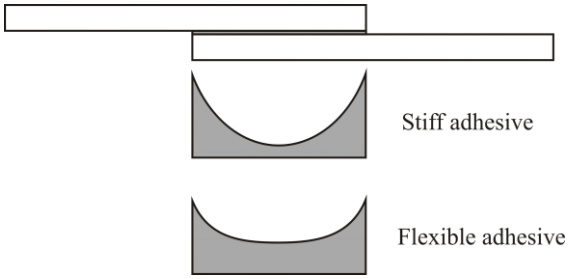

Figure 6 – Shear stress distribution in a single lap joint for different adhesives' behaviour [11]

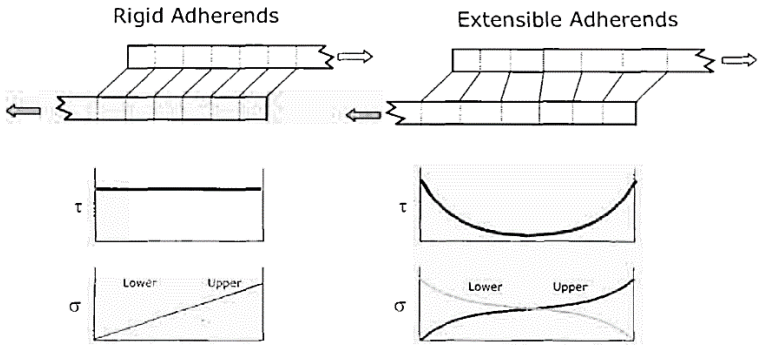

Figure 7 – Shear stress distribution in a single lap joint for different adherends' behaviour [11]

Tensile loads develop when the applied loads are uniformly distributed along the bonded area, perpendicularly to the joint plane. In real applications, it is difficult to guarantee the

exact thickness of the adhesive and, therefore, the loads rarely are purely axial. Thus, the stress distribution in the adhesive joint is not uniform, creating peak peel stresses at the overlap edges [12, 13].

Compressive stresses are related to compressive loads in the adherends. In this case, the stress distribution is uniform along the bonded area, perpendicularly to the adhesive plane (in fact, a bond that is subjected only to compressive loads does not need an adhesive) [12, 14].

Cleavage stresses occur when loads at the overlap edge tend to separate the adherends. The maximum stress occurs at the loaded edge and gradually decreases through the adhesive bond. Cleavage stresses should be minimized whenever possible in adhesive joints, and solutions that are mainly loaded in shear should be consider instead. In butt joints, if the load is not purely axial, cleavage loads have may appear [15].

2.1.4 Failure modes

The main objective of a bonded joint is to transmit loads between two components, keeping its structural integrity under static/dynamic loads and unfavourable environmental conditions. The knowledge of the stress distributions in the adhesive layer and the failure modes is highly important for joint design.

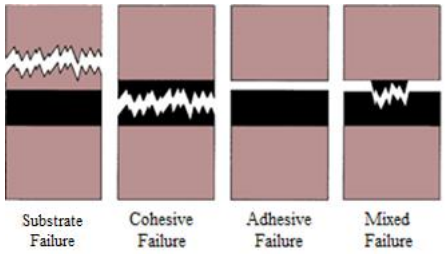

Figure 8 – Possible failure modes in bonded joints [16]

In general, four failure modes can occur in a bonded joint: cohesive failure (inside the adhesive), adhesive failure (at the adherend/adhesive interface), adherend tensile failure and mixed failure. The ideal type of failure is the cohesive, which occurs when the adhesive/adherend interface is higher that the internal strength of the adhesive. A mixed failure occurs when adhesive and cohesive regions alternate across the bond [17, 18]. This

type of failure occurs when the surface preparation is not uniform in the bonding surfaces, including some areas with bad adhesion.

Adherend failure takes place when the internal strength of the adhesive and between the adhesive and adherends are higher than the internal strength of the adherends. In this case, failure occurs in the adherend.

An adhesive failure occurs when there is a failure in the adhesion between the adhesive and one of the adherends and it is normally related with a bad surface preparation

2.1.5 Joint configurations

In a bonded joint, the load is transferred between the adherends by the adhesive. The joint strength depends on the design, the properties of the adhesive and the bond quality. The adhesive joint is more efficient when the adhesive layer is subjected mainly to shear. Bonded joints can be manufactured in many different configurations, as shown in Figure 9. Each type of joint has its own specificities in which regards to manufacturing difficulties, stress distributions and consequently load bearing capabilities.

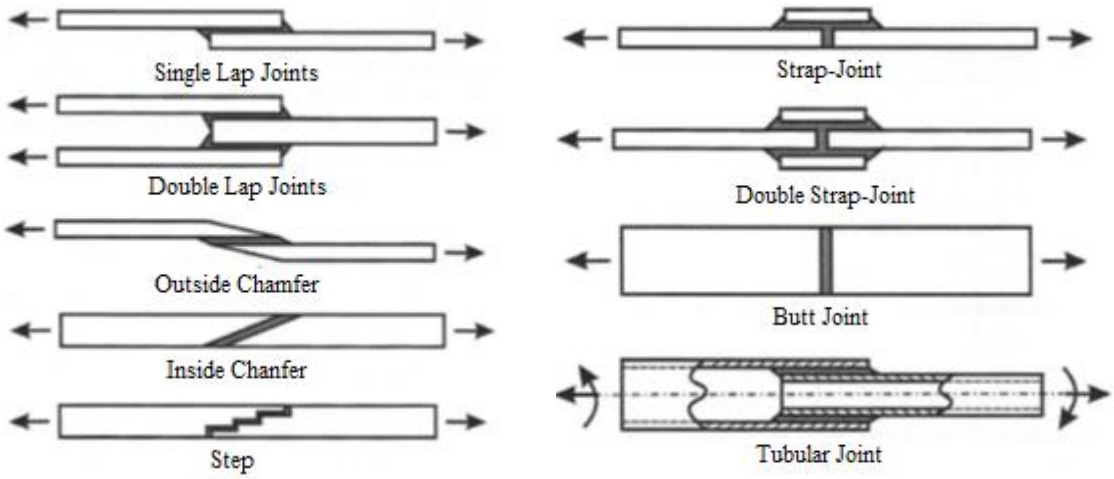

Figure 9 – Different configurations of bonded joints [11]

Due to their simplicity, SLJ are the most common in the literature. But this type of joints is subjected to transverse deflection because of the non collinear load path (Figure 10). The asymmetry of the joint causes bending leading to significant peel stresses (Figure 11) [17].

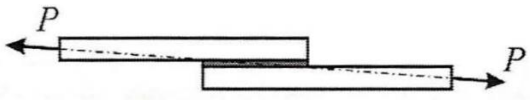

Figure 10 – Non collinear load path [11]

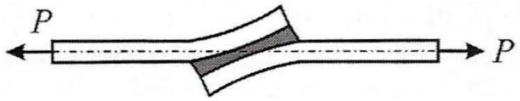

Figure 11 – Joint bending [11]

When the joints need to sustain higher loads, SLJ are not the most recommended. Under these conditions, double lap joints are more efficient. Actually double lap joints are more difficult to manufacture but they can deal with higher loads and less deformation. This type of joint is characterized by two outer adherends at one of the joints sides and an inner adherend in-between. The double lap joint configuration is under shear and peel stresses as well, but the middle adherend is not subjected to flexure. On the other hand, bending moments in the outer adherends develop as shown in Figure 12. As a consequence, the adhesive layer is under peel stresses near the edge of the outer adherends and under compressive normal stresses at the other edge [17].

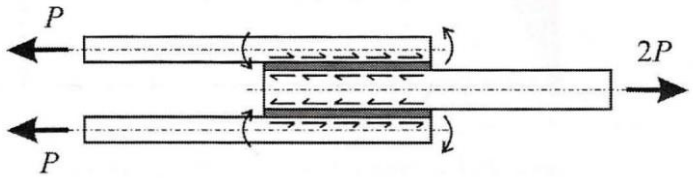

Figure 12 – Transmission of loads in a double lap joint [11]

SLJ with chamfers (Figure 9) at the overlap edges have the same features than the traditional SLJ, but the chamfers on the top reduce the stress concentrations in the adhesive, therefore providing more uniform shear stress distribution [19].

Inside chamfer joints (bisel), as shown in Figure 9, are very efficient because of the tapering effect of the adherends, which turns the stress distribution more uniform, and because the adherends are collinear. The peel and shear stress distributions are practically uniform across the adhesive layer [19].

Butt joints (Figure 9) are not the most common, and this type of joint is commonly limited to test adhesives to tensile and peel loads. Its strength is highly dependent on the bonded area and misalignments to the applied load [19].

Strap joints bond adherends with external elements (patches) are commonly used for repairing and they provide higher strength than the traditional SLJ, but they are more difficult to manufacture. In the industry, using this joining configuration for repairing is particularly attractive over the components' replacement because of the lower costs involved [19].

2.2 Joints between different adherend materials

Adhesive joints are widely used in the aerospace and automotive industries to join dissimilar materials. Adhesive joints provide a more uniform stress distribution over the overlap area and at the same time they weigh less [20]. Adhesives can be used to join a large variety of materials like metal-metal, metal-plastic, metal-composite, metal-ceramic in order to apply the best materials combination for a given application. The stress fields are affected by the different stiffness of the adherends, since it is possible to find different shear and peel stress distribution when using joints between different materials. The increase in the stiffness of the materials promotes lower elastic deformation in the adherends, lower bending rotation of the joints and consequently lower stress concentrations at the edges of the overlap [21].

2.2.1 Metal-to-metal joints

Although new materials like plastics and composites have replaced metals in many industrial products, metals will continue to be used where their unique combination of properties such as high strength, high temperature resistance and low cost is required. There are several ways and combinations to join two metal adherends like mechanical clinching, weld bonding, rivet bonding and adhesive bonding. Adhesives can be combined with mechanical methods in order to increase the static and fatigue strength, and at the same time to reduce the production costs, because these joints do not require fixtures during the cure of the adhesive. The most common adhesives used to joint metal to metal in industry and aerospace applications are epoxy adhesives. When it is necessary to join two metal adherends without a good surface preparation, reactive acrylics are very effective. Cyanoacrylate adhesives are the most

suitable to join quickly two materials. However, they have poor impact strength and low adhesive peel strengths. Alongside the need to join typical metals like steel, light metals such as aluminium alloys are also extensively used in the industry. This material is being increasingly used in aerospace and automotive industries due to the weight saving and good strength to weight ratio. One of the disadvantages of aluminium alloys is the poor torsional and beam stiffness, but this limitation can be overcome by using adhesives [22].

2.2.2 Metal-to-composite joints

Is not common to use mechanical joints in composites. The manufacturing process of the holes result in micro and/or local damage in the composite. Other problems associated to fastening holes and fasteners are the stress concentrations and weight increase. Therefore, adhesive bonding is increasingly being used to join metal to composite materials [23]. Within this scope, some articles concluded that flexible adhesives delay crack initiation and final failures [24]. Another challenge in joining metals to composites is the stiffness and thermal expansion coefficient differences between the materials. The coefficient of thermal expansion of the aluminium is much higher than that of the composite. This difference causes a reduction in strength in the presence of temperature variations. Simultaneously, the composite is much stiffer than the aluminium and, consequently there is a reduction in the load carrying capacity of the joint because of the higher peak stresses in the joints [25].

2.3 Strength prediction of bonded joints

In general, strength and failure predictions of adhesive joints are based on strength of materials, fracture mechanics or damage mechanics approaches. The most relevant techniques are briefly explained in the following subsections.

2.3.1 Continuum mechanics

The continuum mechanics approach consists of using of analytic or numerical methods to obtain the maximum values of stress, strain or strain energy. These values are subsequently compared with the corresponding material allowable mechanical values for assessing failure. Regarding the use of the FE method with this purpose, the maximum principal stresses were

used to predict successfully the strength of adhesive joints with brittle materials. However, in this criterion all the other principal stresses are not considered, even though they are not nil by establishing the failure modes in lap joints bonded with brittle adhesives, Adams et al. [26] have extensively used this criterion to predict joint strength with success. An important detail concerning the stress analysis through numerical methods is the mesh size, because of the stress singularities at the bond extremities that make the stresses mesh dependent.

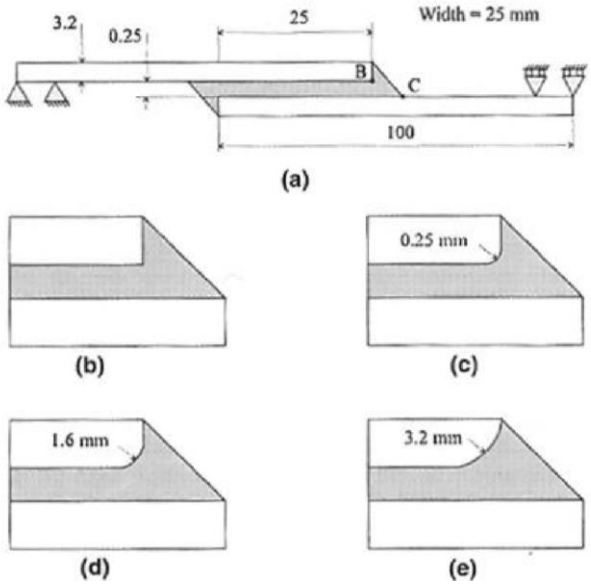

Figure 13 – SLJ with rounded corners [27]

Applying the geometric modifications depicted in Figure 13 (rounded corners) at the overlap edges, a considerable reduction of the peak stresses is attained. This basic change improves the stress distribution, improves the overall joint strength and eliminates the stress singularity, which facilitates the application of a stress or strain criterion [28]. Figure 14 presents the effect of rounded corners in adhesive joints on the maximum principal stresses in the adhesive layer. Due to production process, the adherend corners have small irregularities and therefore this may affect the stress distribution and, consequently, the joint strength. Adams and Harris [28] demonstrated that rounded corners increase the strength of adhesive joints when compared with joints with sharp adherend corners.

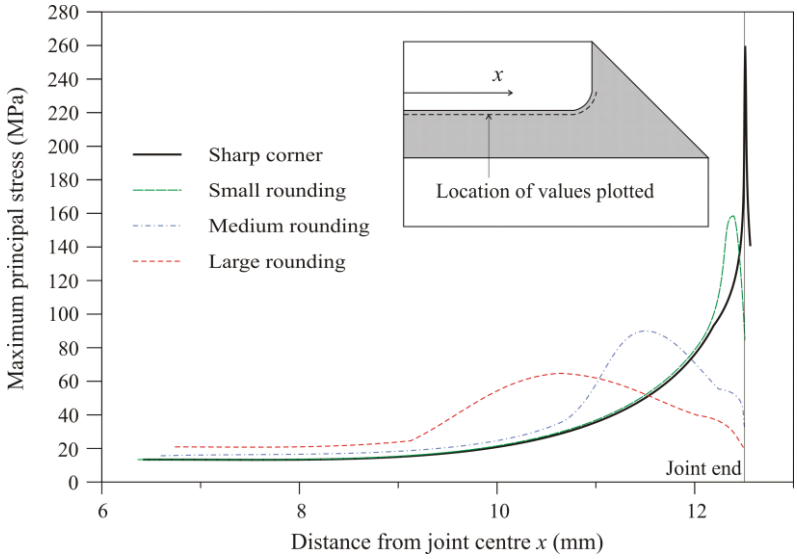

Figure 14 – Variation of the maximum principal stresses with different rounded corners [27]

Other criteria are available to assess failure than the maximum principal stress criteria. The von Mises criterion states that the material fails due to multi-axial stress when the distortion energy reaches a critical value [29], that is

$$\sigma_{VM}^2 = (\sigma_1 - \sigma_2)^2 + (\sigma_2 - \sigma_3)^2 + (\sigma_3 - \sigma_1)^2 = \text{constant.} \quad (1)$$

σ_i (i=1, 2, 3) are the principal stresses. It should be noted that this criterion is more applicable to material yielding than strength. The criteria based on stresses are not appropriate for bonded joints when using ductile adhesives, because when these adhesives start to yield, they continue to bear deformation before complete failure. Under these conditions, strain-based criteria are more suitable. However, the strain values are also affected by the mesh dimensions [30]. Clarke and McGregor [31] at the end of the 20th century verified that is possible to predict the failure of an adhesive bond when the maximum principal stress surpasses the maximum uniaxial strength measured at a certain distance from the singularity. In this criterion, the maximum strength prediction is not significantly affected by the change of the geometry. This method has the disadvantage of requiring the calibration of this characteristic distance for each joint configuration [27].

2.3.2 Fracture mechanics

Cracks are the most common defects in structures and, due to the impossibility of addressing these discontinuities with continuum mechanics, fracture mechanics has been developed

with the purpose of filling this gap. In fracture mechanics, it is well accepted that stresses calculated using continuum mechanics are singular at the crack tip. With current theories on mechanics, such a singularity always exists when the crack angle is less than 180º. This result was found by Williams [32] for stress singularities in a wedged notch. In recent years, fracture mechanics has been applied to many engineering problems, mainly in the aeronautic industry. This method can be also applied in the study of adhesive joints using the strain energy release rate, G, and respective critical value or fracture toughness, G_C [33]. Stress intensity factors are difficult to determinate when the crack grows at or near to an interface. Due to the different materials used in adhesive joints and varying geometries, fracture in the adhesive joints occurs under mixed mode. For mixed mode fracture, failure criteria can be developed similarly to the classical failure criteria, but it is necessary to introduce the fracture surface concept. Various mathematical surface functions have been proposed to fit the experimental results, such as the three-dimensional (3D) criterion [34]:

$$\left(\frac{G_I}{G_{IC}}\right)^{\alpha}+\left(\frac{G_{II}}{G_{IIC}}\right)^{\beta}+\left(\frac{G_{III}}{G_{IIIC}}\right)^{\gamma}=1, \tag{2}$$

Where G_I, G_{II} and G_{III} are the values of G under pure tension, shear and tearing modes, respectively, and G_{IC}, G_{IIC} and G_{IIIC} are the respective values of G_C. The linear energetic criterion ($\alpha=\beta=\gamma=1$) and the quadratic one ($\alpha=\beta=\gamma=2$) are the most used. The parameters have to be chosen according to the type of experiment. The use of a generalized stress intensity factor, analogous to the stress intensity factor in classical fracture mechanics to predict fracture initiation for bonded joints at the interface corners, has also been investigated. In 1988, Groth [35] assumed that initiation of fracture occurs when the stress intensity factor reaches its critical value. Gleich [36] carried out a similar study by calculating the singularity for a range of adhesive thickness values in 2001. These approaches can be applied for the joints that were used to determine the critical stress intensity facture, bur extrapolation to other types of geometries is not generally possible. In the case of materials that deform plastically, the linear elastic fracture mechanics concepts have to be extended into elasto-plastic facture mechanics. The J integral technique is proper to solve these problems [37].

2.3.3 Cohesive zone models

In the late 1950s / early 1960s, the concept of cohesive zone was proposed by Barenblatt and Dugdale to describe damage under static loads at the cohesive process zone ahead of the apparent crack tip [38, 39]. Since then, CZM have been improved to simulate crack initiation and propagation in several failure problems and composite delamination. CZM are based on spring or more typically cohesive elements [40], connecting two-dimensional (2D) or 3D solid elements of structures. One of the advantage of CZM is the possibility and facility to be incorporated in conventional FE softwares to model the fracture behaviour in various materials, including adhesively-bonded joints [41]. CZM are based on the assumption that one or multiple fracture interfaces/regions can be artificially introduced in structures, in which damage growth is allowed by the introduction of a possible discontinuity in the displacement field. The technique consists of the establishment of traction-separation laws (addressed as CZM laws) to model interfaces or finite regions.

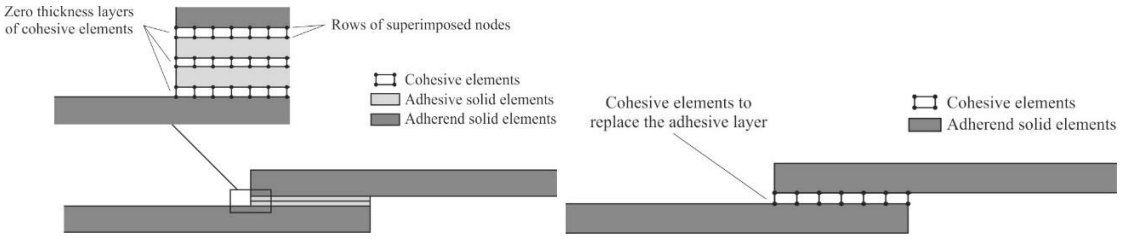

Figure 15 – Cohesive elements to simulate zero thickness failure paths – local approach (a) and to model a thin adhesive bond between the adherends – continuum approach (b) in an adhesive bond [24]

The CZM laws are based on a relationship between stresses and relative displacements and are established between paired nodes of cohesive elements in order to simulate the elastic behaviour up to the cohesive strength and subsequent softening, to model the degradation of material properties up to failure. They can be used to connect superimposed nodes of elements representing different materials or different plies in composites, to simulate a zero thickness interface (local approach; Figure 15 a) [42]), or they can be applied directly between two non-contacting materials to simulate a thin strip of finite thickness between them (continuum approach; Figure 15 b) [43, 44]).

By specifying large scale parameters that rule the crack growth process such as G_{IC}, G_{IIC} or G_{IIIC}, CZM provide a macro-scale reproduction of damage disregarding the microscopic phenomena on the origin of failure [27]. The traction-separation laws are typically represented by linear relations at each one of the loading stages [45]. Figure 16 represents the 2D triangular CZM model actually implemented in Abaqus® for static damage growth, which is detailed here.

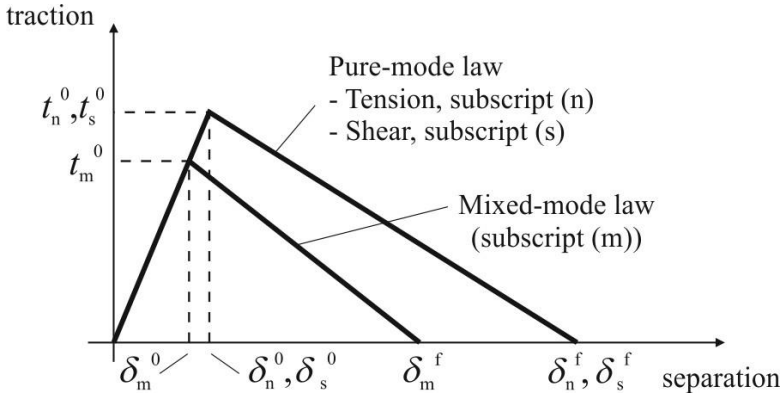

Figure 16 – Triangular traction-separation law available in Abaqus® [46]

The subscripts *n* and *s* relate to pure normal (tension) and shear behaviours, respectively. t_n and t_s are the corresponding current stresses, and δ_n and δ_s the current values of δ. CZM require the knowledge of G_I and G_{II} along the fracture paths and respective values of G_{IC} and G_{IIC}. Additionally, the cohesive strengths must be defined (t_n^0 for tension and t_s^0 for shear), relating to the onset of damage, i.e., cancelling of the elastic behaviour and initiation of stress softening. δ_n^0 and δ_s^0 are the peak strength displacements, and δ_n^f and δ_s^f the failure displacements. The values of δ_n^f and δ_s^f are defined by G_{IC} or G_{IIC}, respectively, as these represent the area under the CZM laws. As for the mixed mode CZM law represented in Figure 16, t_m^0 is the mixed mode cohesive strength, δ_m^0 the corresponding displacement, and δ_m^f the mixed mode failure displacement. Under pure mode loading, the respective t-δ response attains its peak at the cohesive strength (t_n^0 or t_s^0), corresponding to damage initiation by the induced reduction of stiffness of the cohesive element. Softening follows and, when the values of stress are completely cancelled, the crack propagates up to the adjacent set of paired nodes in the failure path, permitting the gradual debonding between crack faces. Under mixed loading, stress and/or energetic criteria are often used to combine the pure mode laws, thus simulating the typical mixed mode behaviour inherent to bonded assemblies. By the mentioned principles, the complete failure response of structures can be

simulated. For the estimation of the cohesive law parameters, a few data reduction techniques are available (e.g. the property determination technique, the direct method and the inverse method) that enclose varying degrees of complexity and expected accuracy of the results [46, 47, 48].

3 Experimental work

This Section addresses the experimental part of the current thesis. First, all the materials and properties of the adhesives and adherends are presented. Next, a brief explanation of the joint geometry and the manufacturing process is made, including the surface preparation of the adherends and techniques that were used to assemble and cure the joints. Finally, the experimental tests and detailed results are exposed and discussed. These results are afterwards compared with the numerical results from Section 4.

3.1 Materials

3.1.1 Adherends

3.1.1.1 Aluminium 6082-T651

The aluminium alloy used for the adherends (Al6082-T651) is commonly used in structural applications. It has good mechanical properties, excellent corrosion resistance and is commonly used for machining. It has the highest strength of the 6000 series alloys. The addition of a large amount of manganese controls the grain structure, which in turn results in a stronger alloy [49]. The aluminium stress-strain (σ-ε) curves are represented in Figure 17, obtained by tensile tests to bulk specimens according to the ASTM-E8M-04 standard. The numerical approximation used in the numerical simulations is also presented. Table 2 describes the 6082-T651 properties [50].

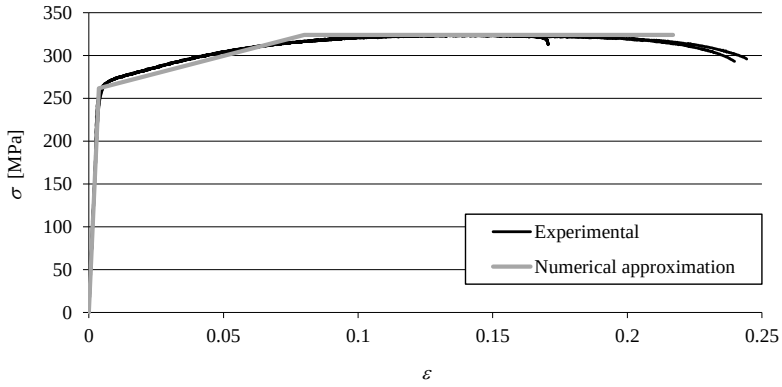

Figure 17 – Aluminium (σ-ε) curves and numerical approximation [50]

Table 2 – Relevant mechanical properties of the aluminium alloy 6082-T651 [50]

Properties	Aluminium 6082-T651
Tensile strength, σ_f [MPa]	324 ± 0.16
Young's modulus, E [GPa]	70.07 ± 0.83
Yield strength, σ_y [MPa]	261.67 ±7.65
Failure strain, ε_f [%]	21.70 ± 4.24
Poisson's ratio, ν *	0.3

* Manufacturer's value

3.1.1.2 Composite Texipreg HS 160 RM

The epoxy pre-preg system used to fabricate the composite adherends is manufactured by SEAL®, consisting of a modified epoxy resin reinforced with high strength carbon fibres in the form of unidirectional tape (0.15 mm thick) [51]. The Texipreg® HS 160 RM elastic orthotropic properties were previously defined [52] and are described in Table 3.

Table 3 – Elastic orthotropic properties of a unidirectional lamina of Texipreg® HS 160 RM (with the fibres aligned in the *x* direction) [52]

Properties	Texipreg® HS 160 RM
E_x [GPa]	109
E_y, E_z [MPa]	8819
ν_{xy}, ν_{xz}	0.342
ν_{yz}	0.380
G_{xy}, G_{xz} [MPa]	4315
G_{zy} [MPa]	3200

3.1.2 Adhesives

Two adhesives from Nagase Chemtex were used in this work, the XNR6852 and the XNRH6823.

3.1.2.1 Nagase Chemtex Denatite XNRH6823

The Denatite XNRH6823 is an epoxy adhesive that is characterized by high strength, easy mixing, excellent sag resistance and excellent water and oil resistance. This structural adhesive is commonly applied in wind blades. This is a two-component epoxy adhesive (XNR6823 as resin and XNH6823 as hardener), which can be applied directly into the surfaces of the adherends and requires curing at 70ºC for four hours. Table 4 describes the properties of this adhesive after curing as defined in the product sheet [53].

Table 4 – Mechanical properties of the Denatite XNRH6823 after curing as defined in the product sheet [53]

Properties	Denatite XNRH6823
Tensile toughness K_{IC} [MPa/m]	1.77
Tensile energy G_{IC} [kJ/m^2]	1.180
Tensile strength [MPa]	57
Tensile modulus [GPa]	2.6
Tensile failure strain, ε_f [%]	7.4

3.1.2.2 Nagase Chemtex Denatite XNR6852

The Denatite XNR6852 is a ductile one-component epoxy adhesive that is characterized by high toughness, good elongation and high peel strength. It is a structural adhesive with typical applications in the automotive industry. This adhesive is directly applied into the surfaces of the adherends and has to be cured at 150ºC for three hours. Table 5 describes the properties of this adhesive after curing as defined in the product sheet [54].

Table 5 – Mechanical properties of the Denatite XNR6852 after curing as defined in the product sheet [54]

Properties	Denatite XNR6852
T_g [C°]	100
Lap-shear strength [MPa]	26
T-Peel strength [N/mm]	200~270
Impact strength [kJ/m^2]	>170
Tensile strength [MPa]	62
Tensile modulus [GPa]	2.6
Tensile failure strain, ε_f [%]	>10

3.2 Joint geometry

The joint geometry and relevant dimensions are shown in Figure 18. The main geometric parameters are the following: overlap length (L_O), adherend length (L_S), length between shims (L_T), adherend thickness (t_S), adhesive thickness (t_A) and specimen width (b).

All the specimens have the same geometry and configuration, varying only L_O and consequently L_s. The remaining parameters are constant. The dimensions of all joint configurations are presented in Table 6.

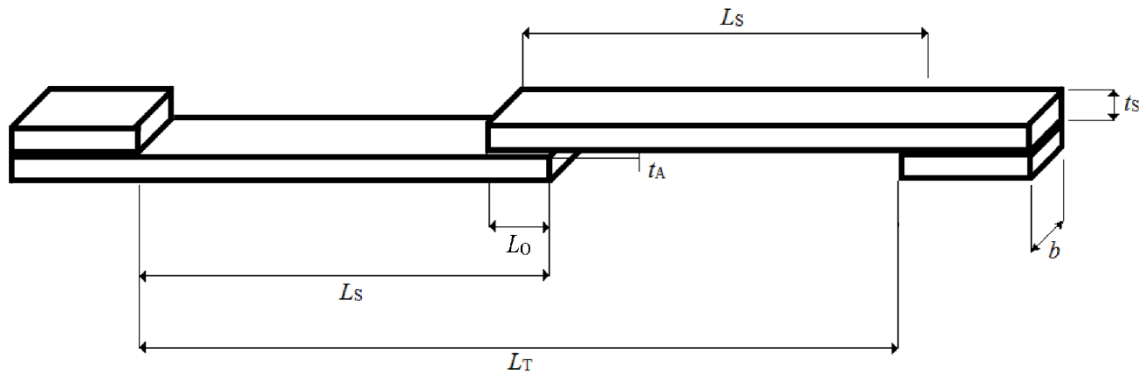

Figure 18 – Geometry configuration [50]

Table 6 – Specimen dimensions [mm]

Overlap length (L_O)	**10**	**20**	**30**	**40**
Adherend length (L_S)	95	100	105	110
Length between shims (L_T)	180	180	180	180
Adherend thickness (t_S)	3	3	3	3
Adhesive thickness (t_A)	0.2	0.2	0.2	0.2
Specimen width (b)	25	25	25	25

3.3 Adhesive joint fabrication

The first step consisted of manufacturing the composite plates to be cut into adherends. With this purpose, three plates were fabricated. From these plates, forty fibre carbon adherends and eighty shims were cut. Alongside, forty aluminium adherends with the same dimensions of the composite adherends were cut from a laminated sheet. The next step consisted of manufacturing the single-lap joints. A total of forty joints was manufactured with four different values of L_O. The last step before manufacturing the adhesive joints was the preparation of the adherends' bonding surfaces, to maximise the adhesive adhesion. Next, the joints were assembled in a jig and cured in hydraulic press machine. After the time necessary to cure the adhesive, the excess adhesive at the bonding area was removed and the joints were then ready for testing. These procedures are described in more detail in the next Sections.

3.3.1 Adherends' fabrication – CFRP and aluminium

Initially, three composite plates with 300×300×3 mm^3 were manufactured. Each plate is composed by twenty pre-preg layers with the same orientation, cut from a continuous pre-peg roll. Before the manual stacking procedure, these layers were initially cut into sheets with 300×600 mm^2 (Figure 19) and then cut in half into sheets with 300×300 mm^2 (Figure 20).

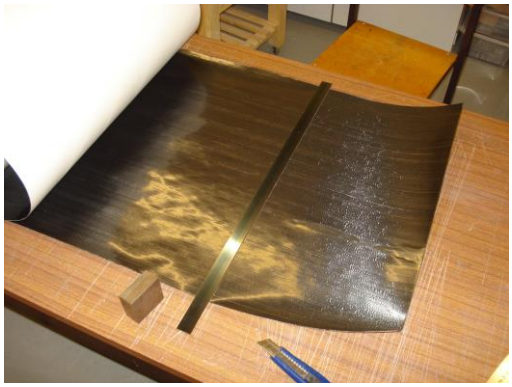

Figure 19 – Sheets with 600×300 mm^2

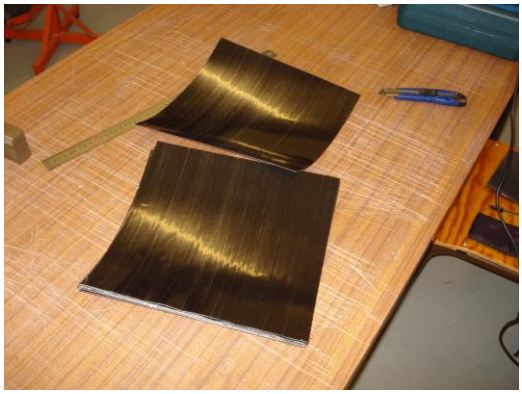

Figure 20 – Sheets with 300×300 mm^2

After cutting, the sheets were individually piled up using a heat gun in order to facilitate the adhesion between sheets (Figure 21) and a steel block to compress the sheets and remove the air bubbles between sheets (Figure 22).

Figure 21 – Heating the sheets with a heating gun

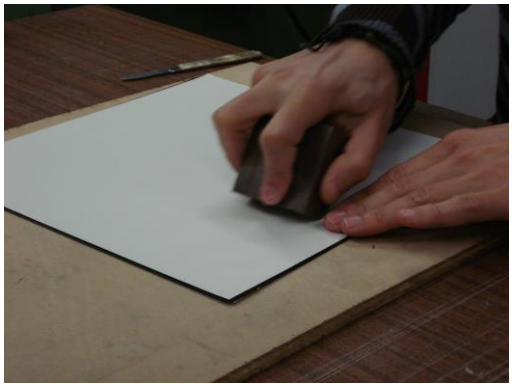

Figure 22 – Removing air bubbles with a steel block

Next, the un-cured plate of 20 stacked sheets was placed in a matrix (Figure 23) and then the complete set placed in the hydraulic press machine to cure the resin. Figure 24 shows a cured composite plate. In total, 3 plates were fabricated.

Figure 23 – Un-cured plate of 20 stacked sheets in the matrix

Figure 24 – Cured plate of CFRP

The curing conditions for the CFRP plates are shown in Figure 25

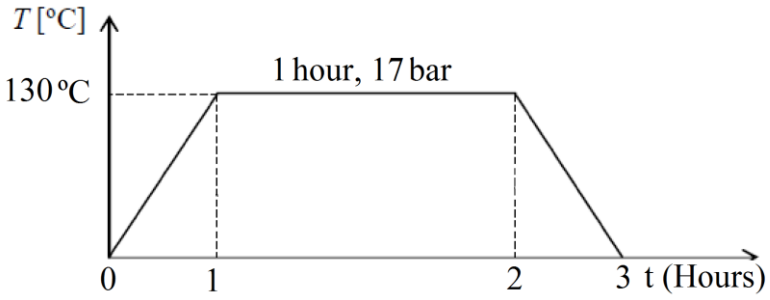

Figure 25 – CFRP plates' curing cycle

The plates were subsequently cut into forty fibre carbon adherends with 25×140×3 mm^3 and eighty shims with 25×25×3 mm^3 using a cutting machine available at *Instituto Superior de Engenharia do Porto*. Alongside, forty adherends of aluminium with the same dimensions of the CFRP adherends were cut from an aluminium plate. Examples of composite and aluminium adherends are presented in Figure 26, and of composite shims are showed in Figure 27.

Figure 26 – Aluminium and CFRP adherends

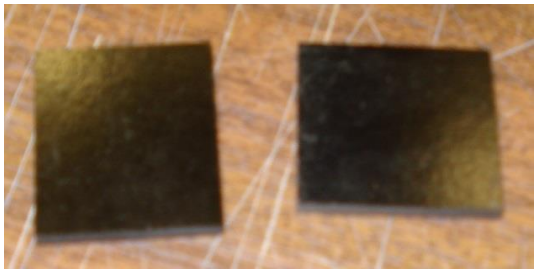

Figure 27 – CFRP shims

3.3.2 Surface preparation

Surface preparation of the adherends is necessary in order to guarantee the proper adhesion between the adherends and the adhesive for optimal results. The technique to be used depends of the material. In this work, two different materials were subjected to surface treatment: the CFRP and aluminium adherends.

3.3.2.1 Aluminium surface preparation

Two techniques were used to prepare the bonding surface of the aluminium adherends. The first one is a mechanical passive process, which consists of removing the oxide layers formed due the exposure to the surrounding environment and increasing the surface roughness. Shot-blasting was considered with this purpose using the equipment available at *Faculdade de Engenharia da Universidade do Porto* (Figure 28). After this process, cleaning is required. The second treatment consists of removing particles and dirt (grease and oil) resulting from the cutting process and particles from the shot-blasting operation. The cleaning process is considered a chemical passive process, and acetone was used with this purpose. The final appearance of the aluminium adherends can be seen in Figure 29.

Figure 28 – Shot-blasting machine

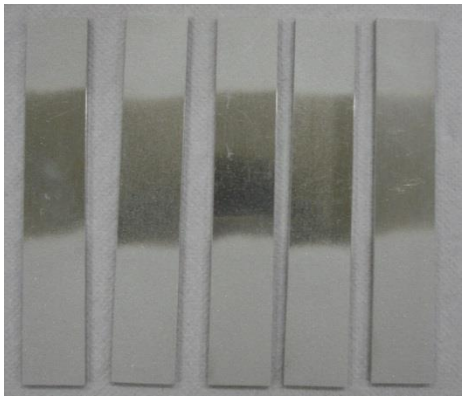

Figure 29 – Aluminium adherends after surface preparation

3.3.2.2 Composite surface preparation

The surface preparation processes used for the composite adherends are identical to those used for the aluminium, only changing the respective procedure. Due to the material involved, shot-blasting cannot be used and the mechanical passive process has to be applied manually, using manual abrasion with sandpaper (Figure 30). The chemical passive process was applied identically to the aluminium adherends. Figure 31 shows the final result of the surface preparation.

Figure 30 – Manual abrasion process with sandpaper

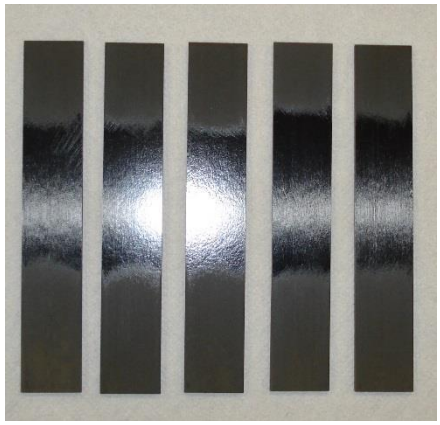

Figure 31 – CFRP adherends after surface preparation

3.3.3 Joint fabrication

All the joints were manufactured using a jig available at *Faculdade de Engenharia da Universidade do Porto* (Figure 32). This jig has several alignment pins that enable the simultaneous production of five specimens and thereby ensured the dimensional standardization of all specimens. In order to guarantee the adhesive thickness and total length of the specimens, spacers were used. Initially, mould release agent was applied on all relevant jig surfaces to facilitate the extraction of the specimens. Next, the aluminium adherends and spacers were inserted between the pins (Figure 33).

Figure 32 – Jig with alignment pins

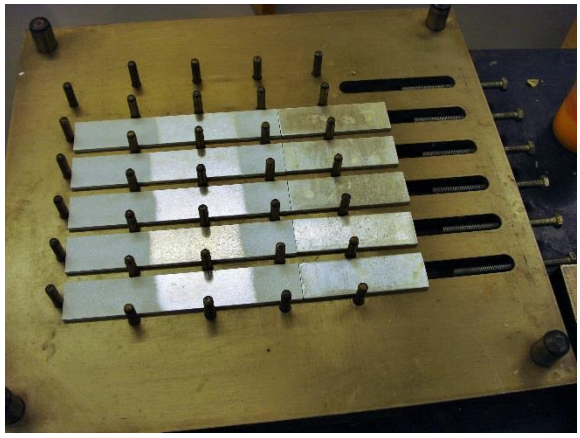

Figure 33 – Jig with aluminium adherends and spacers

Following, the adhesive was applied on the bonding surfaces that were already treated (Figure 34). To ensure the desired value of t_A, spacers were placed between the adherends and the shims in order to raise the CFRP adherend by 0.2 mm from the aluminium adherend. As the final step, the CFRP adherend was placed above the spacers (Figure 35).

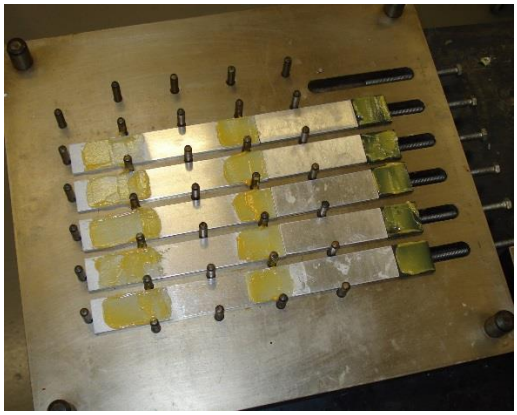

Figure 34 – Adhesive placed on the aluminium adherends' bonding surfaces and CFRP shims

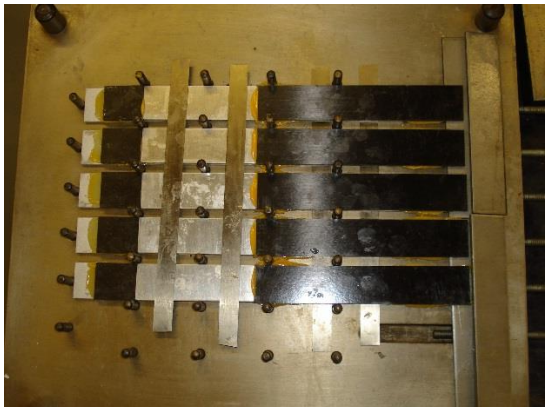

Figure 35 – CFRP adherends and spacers placed above the aluminium adherends

The jig was placed inside a hydraulic press machine in order to cure the adhesive (Figure 36). After the curing time was completed (depending of the adhesive), the jig was removed from the hydraulic press machine and the specimens were carefully removed from the jig (Figure 37).

Figure 36 – Hydraulic press machine

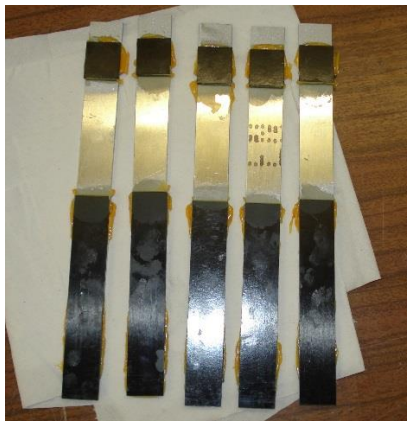

Figure 37 – Specimens after the curing process

The curing conditions for the joints bonded with the adhesive XNR6852 and XNRH6823 are described in Figure 38 and Figure 39, respectively.

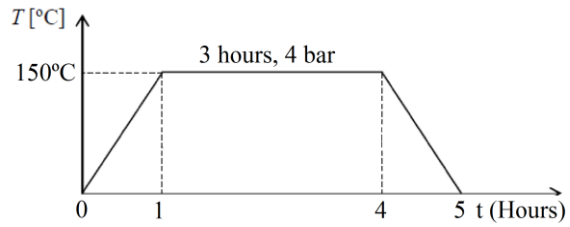

Figure 38 – XNR6852 curing cycle

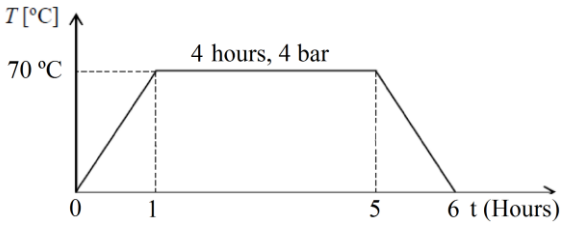

Figure 39 – XNRH6823 curing cycle

Due to the pressure applied to the joints, the adhesive spread to the outside of the bonding area, as it can be seen in Figure 37. This adhesive excess has to be removed to provide the ideal joint configuration depicted in Figure 18. This was carried out manually using a Dremel® machine (Figure 40). The final appearance of the specimens is presented in Figure 41.

Figure 40 – Dremel® Machine [55]

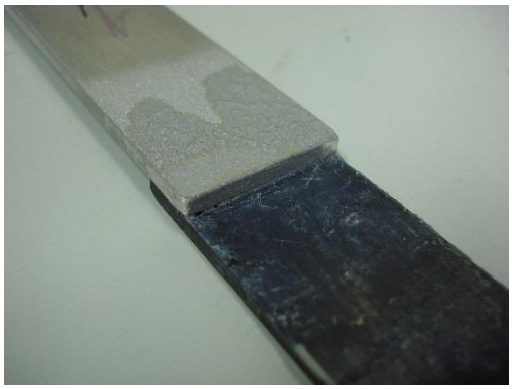

Figure 41 – Specimen after removing the adhesive excess

At the end, forty joints with four different values of L_O were manufactured. Ten specimens were fabricated with each L_O value: five with the brittle adhesive Denatite XNRH6823 and five with the ductile adhesive Denatite XNR6852.

3.4 Experimental testing

After the specimens' manufacturing, the next step was the experimental testing. All the experiments were carried out in an Instron® 3367 testing machine (Figure 42), available at

Faculdade de Engenharia da Universidade do Porto, with a displacement rate of 0.5 mm/min, considering a distance between grips of 180 mm (equal to the value of L_T) and at room temperature. Figure 43 shows as example one specimen being tested.

Figure 42 – Testing machine Instron® 3367

Figure 43 – Specimen being tested

3.5 Results

In this Section, the failure modes, load-displacement (*P-δ)* curves obtained from the experimental tests and a brief analysis of the joint strength are discussed for the joints bonded with the two adhesives.

3.5.1 Failure modes

Due to using adhesives with different ductility and values of L_O, different failure modes can occur in view of using CFRP adherends that are prone to delaminate [56]. In this case, the type of adhesives has been prevalent to the type of failure that occurred. Oppositely, the variation of L_O showed no influence on the failure mode. In Figure 44 and Figure 45, a single specimen for each L_O value is presented as an example for the XNRH6823 and XNR6852, respectively, with increasing L_O values from left to right (10 mm to 40 mm).

Figure 44 – Failure modes of the specimens manufactured with the brittle adhesive (XNRH6823)

By visual inspection of the specimens manufactured with XNRH6823 (Figure 44), it is possible to conclude that all failures where a mix of delamination with adhesive failure. For the joints with all values of L_O, failure starts at the edge of the aluminium adherend as adhesive failure and then shifts to an intralaminar failure. It should be mentioned that failure of the specimen in Figure 44 with L_O=30 mm may visually seem an adhesive failure, but a close visual inspection shows that the failure is actually intralaminar. All the failures occurred at approximately 0.05 mm from the adhesive layer, which was testified used a digital calliper to determine the distance to the adherend face where the intralaminar failure occurred.

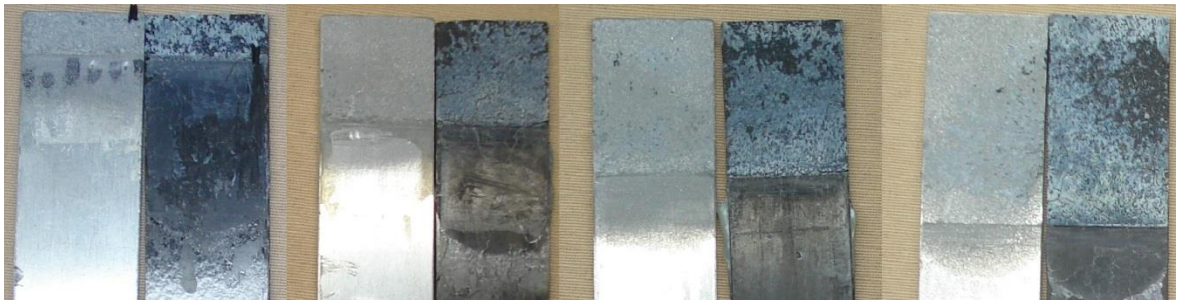

Figure 45 – Failure modes of the specimens manufactured with the ductile adhesive (XNR6852)

After performing the experimental tests with the specimens manufactured with the XNR6852, all failures where cohesive in the adhesive layer (Figure 45). In contrast to the XNRH6823, the composite adherends were left intact after the tests, without any signs of damage or delamination. For the specimens with L_O=30 and 40 mm, the aluminium adherends suffered plastic deformation.

3.5.2 *P-δ* curves

Figure 46 and Figure 47 present the valid *P-δ* curves of the joints bonded with the brittle adhesive (XNRH6823) and the ductile adhesive (XNR6852), respectively. Due to some manufacturing issues, the experimental results of few joints were markedly different from the average behaviour and, therefore, those results were excluded from the analysis.

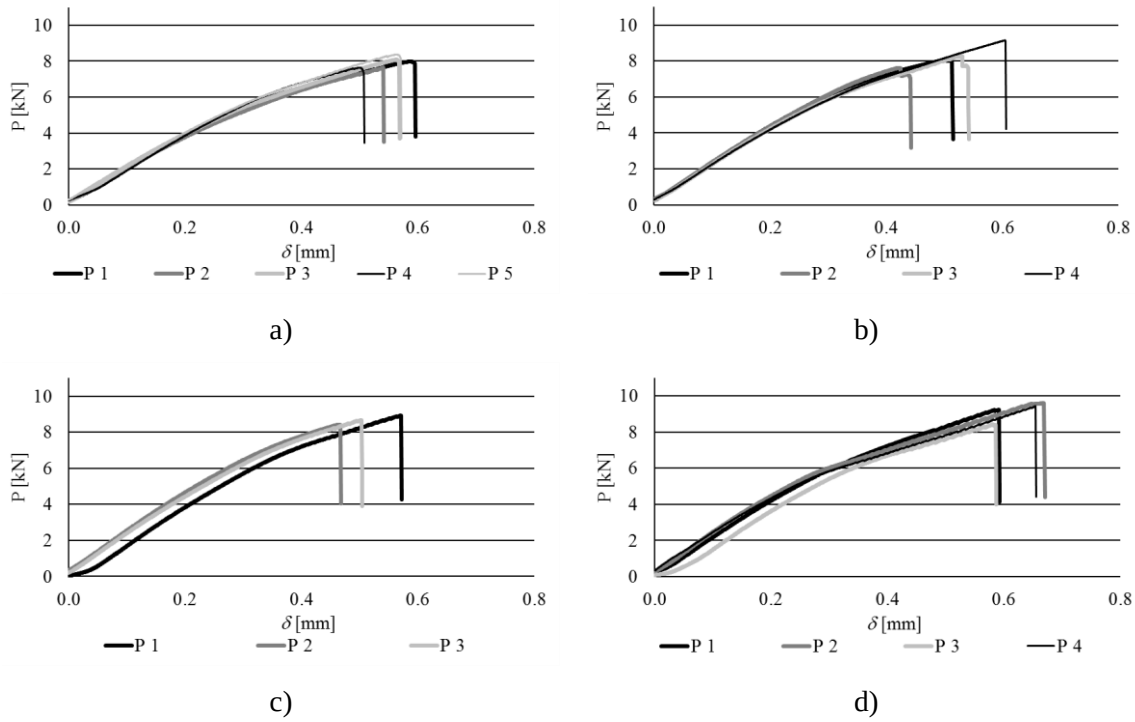

Figure 46 – Experimental *P-δ* curves obtained using the adhesive XNRH6823: L_O=10 mm (a), L_O=20 mm (b), L_O=30 mm (c) and L_O=40 mm (d)

For each adhesive and value of L_O, the curves have a similar behaviour in which pertains to the load evolution up to the maximum load (P_m), failure displacement and value of P_m, although showing some fluctuations in P_m. In the joints bonded with XNR6852, the evolution of P_m with L_O is highly nonlinear. The first drop of stiffness at approximately 7000 N is related to the onset of the adhesive layer's plasticization, and the steady-state value of P attained for the joint with L_O=40 mm at approximately P=22000 N is due to plasticization of the aluminium adherends. A more detailed analysis of the P_m values will be performed in the next Section.

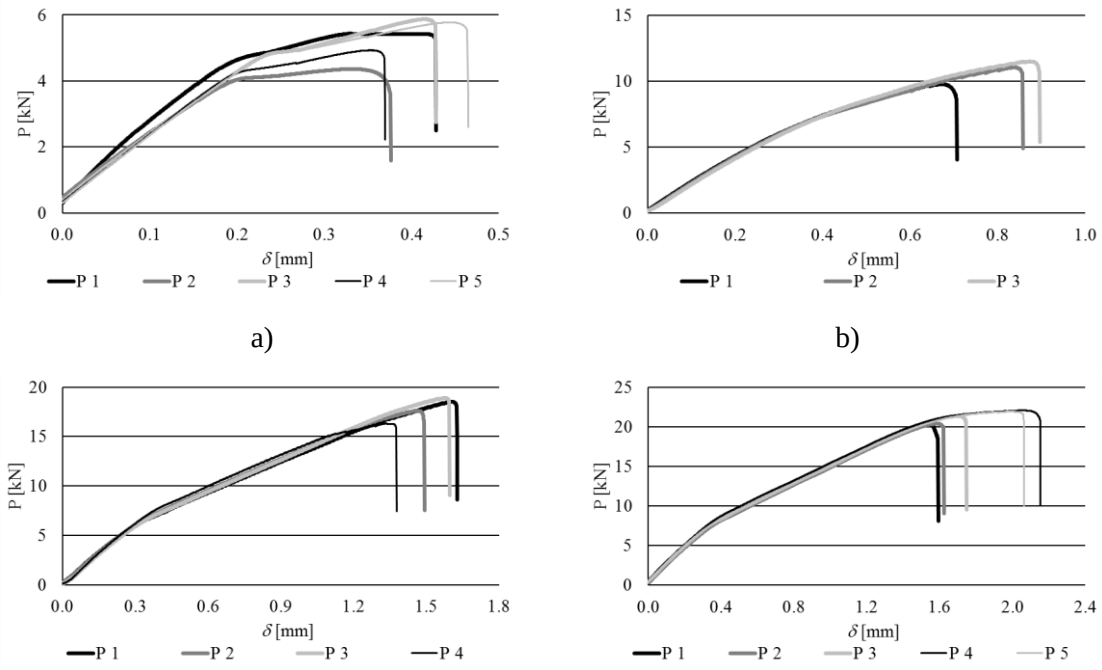

Figure 47 – Experimental *P*-δ curves obtained using the adhesive XNR6852: L_O=10 mm (a), L_O=20 mm (b), L_O=30 mm (c) and L_O=40 mm (d)

3.5.3 Joint strength

The average value of P_m and corresponding deviation for each L_O value is shown in Table 7 for the XNRH6823 and Table 8 for the XNR6852. The individual percentile deviation between each specimen and the average value of P_m for the same L_O/adhesive configurations is also presented. The specimens with more than 10% difference from the average typically were not considered in the analysis. An exception was made for the joints bonded with the XNR6852 for L_O=10 mm, as it will be explained further.

Table 7 presents the analysis for the XNRH6823. The evolution of P_m with L_O is practically linear and the results between specimens of the same L_O value have a good repeatability. However, the increase of L_O does not increase P_m by a significant amount. For L_O=10 mm, all the specimens had a deviation under 5% from the average and all tested specimens were considered in the analysis. For L_O=20 mm, one specimen was removed, and the scatter between specimens was the highest of all L_O values. For L_O=30 mm, two specimens were removed from the analysis, and the percentile difference of the remaining specimens was under 3%. For L_O=40 mm, one specimen was removed, with the percentile difference under 7%.

Table 7 – P_m and deviation for the joints bonded with XNRH6823

L_O [mm]		10	20	30	40
Average P_m (N)		7 937.12	8 273.99	8 672.07	9 172.30
Standard deviation		309.48	646.45	247.65	519.17
Specimens	1	3.88%	8.04%	2.78%	5.62%
	2	4.05%	8.49%	2.94%	5.41%
	3	3.83%	7.80%	2.86%	6.16%
	4	4.06%	7.06%		5.51%
	5	3.70%			

Table 8 presents the statistical analysis for the joints bonded with XNR6852. The higher plasticity of the XNR6852 enables a significant increase of P_m with the increase of L_O. As referred before, for L_O=10 mm an exception was made because all the specimens were above 10% of the average P_m value and, for that reason, all the specimens were considered in the analysis. For L_O=20 mm, two specimens were removed from the analysis and, as seen in the joints bonded with XNRH6823, this L_O value had the highest percentile difference when compared with the other L_O values. In the analysis of the joints with L_O=30 mm, one specimen was removed and the percentile difference was under 6%. For L_O=40 mm, all the specimens were considered and the lowest percentile difference was found, (under 4%).

Table 8 – P_m and deviation for the joints bonded with XNR6852

L_O [mm]		10	20	30	40
Average P_m (N)		5 274.65	10 904.76	17 322.71	21 217.30
Standard deviation		629.86	669.03	958.90	803.62
Specimens	1	11.59%	6.06%	5.18%	3.95%
	2	14.44%	5.82%	5.44%	3.94%
	3	10.73%	6.57%	5.87%	3.76%
	4	12.77%		5.70%	3.64%
	5	10.90%			3.67%

Figure 48 shows the comparison of the average P_m values and respective deviation of the two adhesives for the different values of L_O. A more detailed analysis of the evolution of P_m with L_O for both adhesives, enables concluding that the adhesive has a major influence on the joints' behaviour. Increasing the value of L_O did not reflect on a significant strength improvement for the brittle adhesive (XNRH6823). As it can be seen in Figure 48 a), for this adhesive the average value of P_m increased from approximately 7900 N in the specimens with L_O=10 mm to 9100 N in the specimens with L_O=40 mm. This can be explained by the observed failure in the composite rather than in the adhesive, due to the high strength of the adhesive.

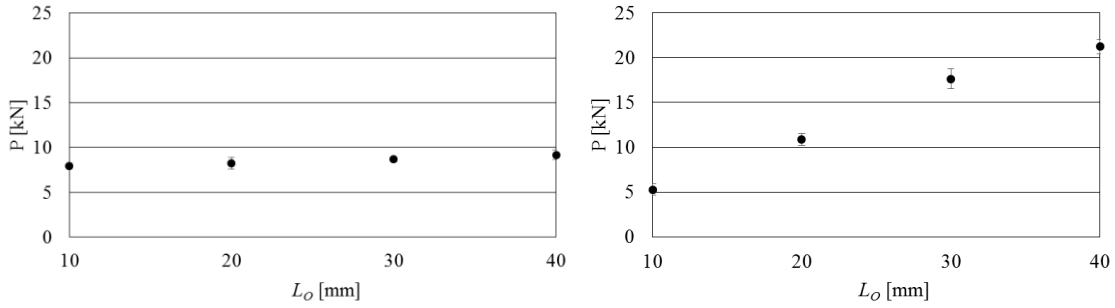

a) b)

Figure 48 – Comparison between the average values of P_m and standard deviation for the adhesive XNRH6823 (a) and for the adhesive XNR6852 (b)

The ductile adhesive (XNR6852) reached higher P_m values when compared to the brittle adhesive (XNRH6823) and, as mentioned earlier, the failure modes were different. Due to the lower mechanical properties of the XNR6852 comparatively to the XNRH6823, the joints bonded with the XNR6852 failed cohesively in the adhesive layer. Because of this and the high ductility of this adhesive, increasing the values of L_O showed large improvements in P_m, with an approximately linear evolution of P_m with L_O. In fact, the evolution of P_m and L_O are nearly proportional: increasing L_O by four times (from L_O=10 mm to L_O=40 mm) causes a P_m increase of about four times. For L_O=10 mm, the average value of P_m was approximately 5200 N, while for L_O=40 mm this value reached approximately 21200 N (Figure 48 b). These behaviour will be detailed in the numerical work after having performed stress and damage variable analyses, for a better perception of all phenomena involved.

Comparing the two adhesives, the XNRH6823 provides better results in the specimens with L_O=10 mm. As average, the joints manufactured with the XNRH6823 presented a value of P_m of 7937±309 N compared to 5274±629 N for the XNR6852. However, with the increase of L_O, the XNR6852 gradually demonstrated to be more effective than the XNRH6823 in this specific joint configuration.

4 Strength prediction

This Section presents all the information related with the numerical conditions, CZM model and results that were obtained using the software Abaqus®. More specifically, initially, a through-thickness normal (σ_y) and shear (τ_{xy}) stress analysis is performed, followed by a damage variable analysis, description of the failure modes, *P*-δ curves and finally the strength prediction. A comparison of the predicted strength is performed with the experiments, and the obtained results are discussed and explained as a function of the stress distributions and damage analysis. This analysis aims at presenting a detailed discussion of the joints' behaviour and a comparative evaluation between different adhesives and values of L_O based on the mentioned information, to provide design principles for hybrid joint design.

4.1 Numerical conditions

The Abaqus® software was used to perform the numerical analysis. This software has an embedded CZM modelling package, such that CZM elements can be coupled with the traditional continuum elements. The simulations consisted of a 2D and geometrically non-linear analysis. The composite and aluminium adherends were modelled as elastic orthotropic and elastic-plastic isotropic, respectively. For the stress analysis, the adherends and adhesive layer were modelled by 4-node plane-strain elements (Figure 49). For the damage and strength analyses, and in order to simulate a composite failure at a specific distance from the adhesive/composite interface, the adhesive layer and the composite failure were simulated by 4-node cohesive elements (Figure 50). In both cases, the triangular mixed-mode CZM available in Abaqus® was used. The adhesive layer was modelled with a single row of cohesive elements. For the composite, the possibility of interlaminar and intralaminar

failures was included by a CZM propagation path located at a distance of 0.15 and 0.05 mm, respectively, from the adhesive layer/composite interface.

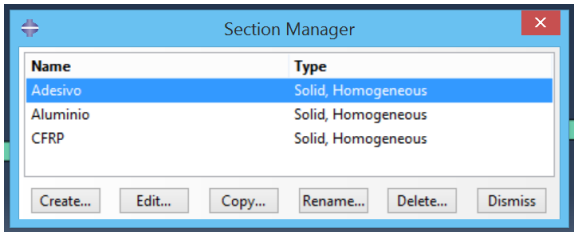

Figure 49 – Abaqus® section manager (stress analysis)

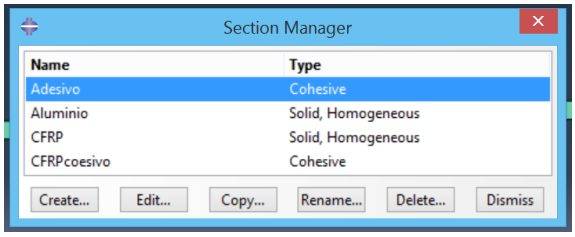

Figure 50 – Abaqus® section manager (damage and strength analyses)

Two types of meshes were constructed depending of the type of analysis: stress or damage/strength prediction. For the stress analysis, a higher degree of refinement was applied to accurately account for the stress variations along the joint, especially at the overlap edges [48]. For the damage/strength analysis, a coarser mesh was used, but considering the minimum refinement required to assure mesh independent results [57].

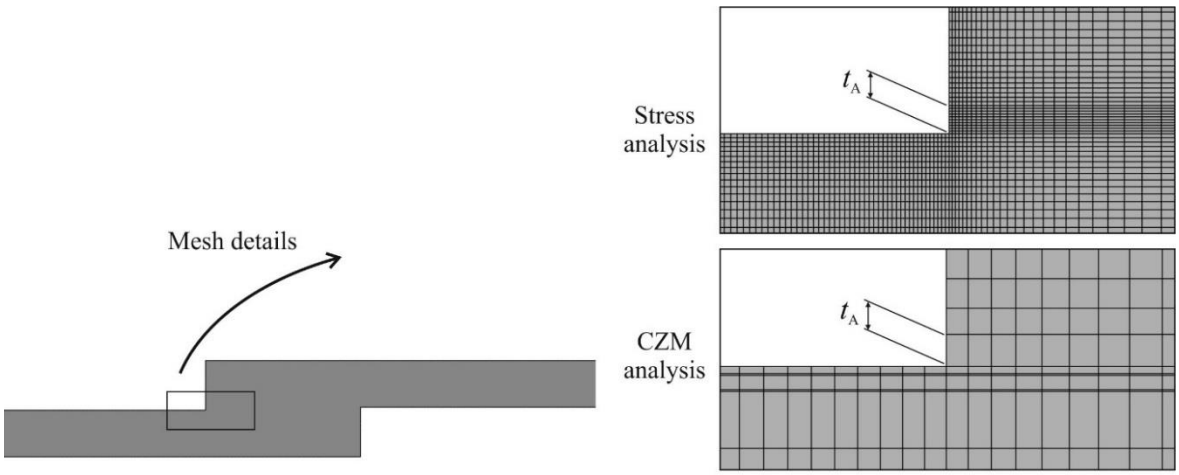

Figure 51 – Example of FE mesh for L_O=10 mm, including mesh details for the stress and damage/strength analyses.

In both cases, mesh grading was applied, with a higher refinement near the overlap edges and in the adherends in the direction of the adhesive to account for the expected stress variations at these locations. Between different L_O values, to provide identical modelling conditions, the size of the FE elements in all models was fixed at the overlap edges (0.02×0.02 mm elements for the stress analysis and 0.2×0.2 mm elements for the damage/strength analysis). The mesh details in Figure 51 express the difference between the

two types of models. Table 9 and Table 10 present the different mesh sizes for all values of L_O at the edges highlighted in red for the stress and damage/strength analyses, respectively.

Table 9 – Mesh refinement for the stress analysis

	L_O [mm]			
	10	20	30	40
Number of elements	75	150	225	300
Bias ratio	20	20	20	20
				
Number of elements	30	30	30	30
Bias ratio	7	7	7	7
				
Number of elements	300	300	300	300
Bias ratio	40	40	40	40
				

Table 10 – Mesh refinement for the damage/strength analysis

	Lo [mm]			
	10	20	30	40
Number of elements	40	80	120	160
Bias ratio	3	3	3	3
				
Number of elements	10	10	10	10
Bias ratio	3	3	3	3
				
Number of elements	160	160	140	140
Bias ratio	10	10	10	10
				

In the adhesive layer length, bias effects were considered with double bias from the central region to the overlap ends, as it can been seen in Figure 52.

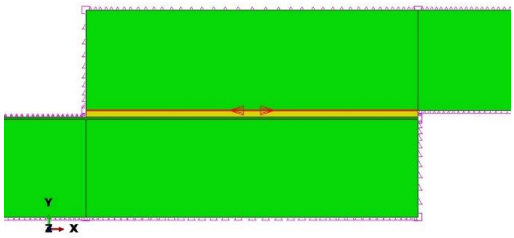

Figure 52 – Bias effects in the adhesive layer length

Bias effects were also considered in the adherends height direction towards the adhesive layer (Figure 53).

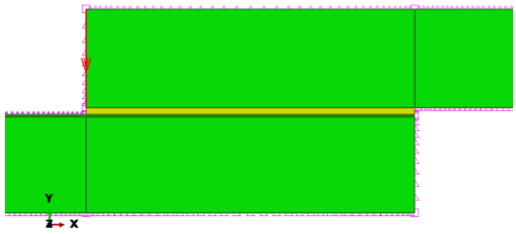

Figure 53 – Bias effects in the adherend's height direction

Along the adherends un-bonded length, bias effects were introduced in the direction of the overlap region (Figure 54).

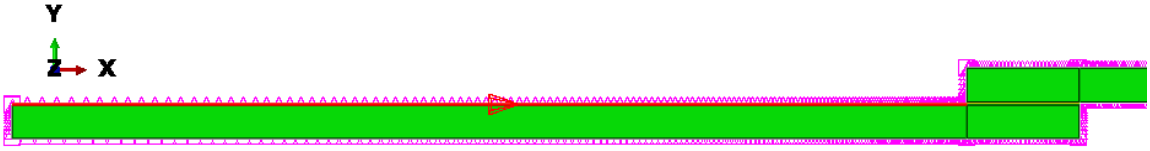

Figure 54 – Bias effects in the adherend un-bonded length

Boundary conditions were considered in order to simulate a tensile test and consisted of clamping the joints at one of the edges, and tensile pulling together with transverse restraining at the opposite edge (Figure 55).

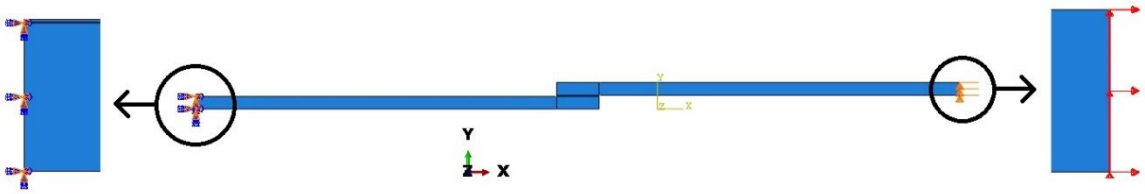

Figure 55 – Boundary conditions applied in the numerical models

4.2 Cohesive zone modelling

As previously mentioned, CZM are based on a relationship between stresses and relative displacements, connecting paired nodes of the cohesive elements to simulate the elastic behaviour up to the cohesive strength and subsequent softening, to model the degradation of material properties up to failure [44].

4.2.1 Triangular cohesive zone model

The triangular CZM law, described in detail in this Section, is the most commonly used due to its simplicity, reduced number of parameters to be determined, and generally acceptable results for most real conditions [58]. However, generically speaking, the shape of the cohesive laws can be adjusted to conform to the behaviour of the material or interface they are simulating for more precise results [59]. The current Section describes the static triangular CZM implemented in Abaqus® v6.14 (Figure 56). Different shape CZM are based on this formulation, typically differing on the softening simulation.

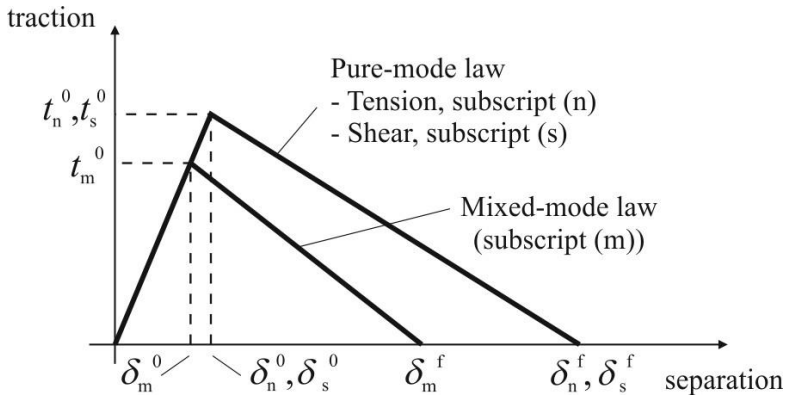

Figure 56 – Triangular CZM law (adapted from [60]).

Under pure mode, damage propagation occurs at a specific set of paired nodes when the values of t_n or t_s are released in the respective CZM law. Under mixed mode, stress and energetic criteria are often used to combine tension and shear [56]. Cohesive elements are assumed to be under one direct component of strain (tension) and one transverse shear strain, which are computed directly from the element kinematics. The membrane strains are assumed as zero, which is appropriate for thin and compliant bonds between stiff adherends. Undamaged strength evolution is defined by a constitutive matrix relating the current stresses, **t**, and strains, **ε**, in tension and shear across the cohesive elements (subscripts n and s, respectively) [60]

$$\mathbf{t} = \begin{Bmatrix} t_n \\ t_s \end{Bmatrix} = \begin{bmatrix} K_{nn} & K_{ns} \\ K_{ns} & K_{ss} \end{bmatrix} . \begin{Bmatrix} \varepsilon_n \\ \varepsilon_s \end{Bmatrix} = \mathbf{K_{COH}} \boldsymbol{\varepsilon}. \tag{3}$$

The matrix $\mathbf{K_{COH}}$ contains the stiffness parameters of the adhesive bond, whose definition depends of whether the local or continuum approach is being used. In the local approach, used to simulate zero thickness fractures, the $\mathbf{K_{COH}}$ parameters are chosen as an extremely

large value (penalty function method) for the cohesive elements not to interfere with the structure deformations, given that this task is to be performed solely by the continuum FE elements [61]. For continuum CZM modelling of bulk thin strips and more specifically for adhesive bonds, a suitable approximation is provided with $K_{nn}=E$, $K_{ss}=G$, $K_{ns}=0$ [60]; E and G are the longitudinal and transverse elastic moduli, respectively. Under these conditions, the model response for the adhesive bond accurately reproduces its deformation behaviour. A few user implemented models in the literature [56] specify equation (3) directly in terms of **t-δ** relationship; **δ** representing the vector of relative displacements including δ_n and δ_s. With this formulation, K_{nn} and K_{ss} are defined as the ratio between E or G and t_A.

Damage initiation under mixed mode conditions can be specified by different criteria. In this work, the quadratic nominal stress criterion for the initiation of damage was used, previously tested for accuracy [59], expressed as [60]

$$\left\{\frac{\langle t_n \rangle}{t_n^0}\right\}^2 + \left\{\frac{t_s}{t_s^0}\right\}^2 = 1. \tag{4}$$

$\langle\ \rangle$ are the Macaulay brackets, emphasizing that a purely compressive stress state does not initiate damage. After t_m^0 is attained (Figure 56) by the fulfilment of equation (4), the material stiffness initiates a softening process. This is simulated by the energy being released in a cohesive zone ahead of the crack tip fracture process zone. This region is where the material undergoes damage by different ways [62], e.g. micro-cracking, extensive plasticity and fibre bridging (e.g. for composite adherends). Numerically, this is implemented by a damage parameter whose values vary from zero (undamaged) to unity (complete loss of stiffness) as the material deteriorates. Complete separation (δ_m^f in Figure 56) is predicted by a linear power law form of the required energies for failure in the pure modes [60]

$$\frac{G_I}{G_{IC}} + \frac{G_{II}}{G_{IIC}} = 1. \tag{5}$$

4.2.2 Cohesive properties determination

Table 11 presents the interlaminar and intralaminar cohesive properties of the pre-preg SEAL® Texipreg HS 160 RM and the relevant mechanical properties of these adhesives. The adhesives were characterized regarding the elastic moduli in tension and shear (E and G,

respectively), the failure strengths in tension and shear (corresponding to t_n^0 and t_s^0) and the values of G_{IC} and G_{IIC}. Bulk tests were performed to characterize the adhesives in tension and Thick Adherend Shear Tests were chosen for shear characterization. Although the cohesive strengths of thin adhesive layers and the bulk strengths of adhesives can differ, since thin layers are constrained between the two adherends and damage growth occurs under mixed-mode [63], in this work the cohesive strengths of the adhesives were assumed as equal to their bulk quantities as an approximation [56]. The values of G_{IC} and G_{IIC} were estimated by Double-Cantilever Beam and End-Notched Flexure tests, respectively, using a robust data reduction method. The large difference between G_{IC} and G_{IIC} observed in Table 11 for the XNR6852 is typical of ductile structural adhesives, which show a significantly larger plastic flow in shear than in tension [64].

Table 11 – Cohesive properties of the adhesives and CFRP

	E [MPa]	G [MPa]	t_n^0 [MPa]	t_s^0 [MPa]	G_{IC} [N/mm]	G_{IIC} [N/mm]
XNRH6823	2600	1000	57	32.9	1.18	2.36
XNR6852	2235.5	859.8	48	20.5	2	4.4
CFRP	10000	10000	25	25	0.18	0.5

4.3 Stress analysis

The stress analysis is based on the study of σ_y and τ_{xy} stresses in the elastic stages of loading. In order to simplify the analysis of the stress distributions two normalizations have been made. The first one consisted of dividing σ_y and τ_{xy} stresses by τ_{avg}, the average shear stress along the overlap for the respective value of L_O. In the second ones, L_O was normalized according to equation (6), where $0 < x/L_O < 1$ is the normalized position along the joint. x/L_O=0 and 1 are the overlap edges and negative x values refer to the un-bonded length of the CFRP. For both σ_y and τ_{xy} stresses, only the region $-0.2 \leq x/L_O \leq 1$ is shown in the stress plots, since further within the composite these stresses are negligible.

$$\frac{x}{L_O} = \frac{x'}{L_O} - \frac{L_S - L_O}{L_O} \tag{6}$$

Figure 57 is a scheme showing the result of the normalization procedure. The black zone represents the composite, the grey zone the aluminium and the red zone the adhesive.

Figure 57 – Schematic representation of the normalized L_O

The stress analysis was initially performed at different planes in the joint for L_O=10 mm and, afterwards, stresses are compared at the adhesive mid-thickness between the four L_O values considered in this study. The considered planes are the following (Figure 58): P1 and P2 - composite layer at 0.15 mm and 0.05 mm from the adhesive layer, respectively, P3 - CFRP/adhesive interface, P4 - adhesive mid-thickness and P5 - aluminium/adhesive interface. The planes in the CFRP layers were accounted for a better perception of the failure modes, including the intralaminar failure observed in the brittle adhesive.

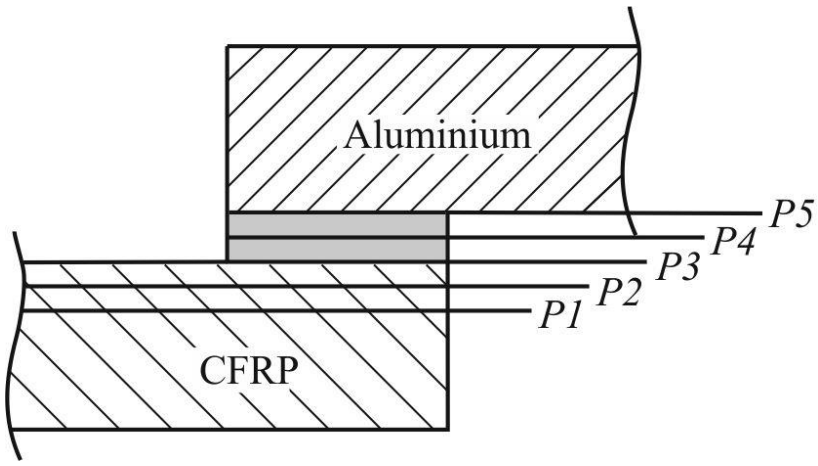

Figure 58 – Horizontal planes considered for the stress analysis

Results are only presented for the joints bonded with the XNR6852, because of the similarity of stress plots between the two adhesives. Actually, the elastic stress distributions and respective stress gradients are determined by the elastic properties of the adhesives [6] and, as shown in Table 11, these are almost identical for the adhesives under analysis.

4.3.1 Peel stresses

In this section, σ_y stress distributions are analysed at all different planes in the joint for L_O=10 mm and, following, σ_y stresses will be considered at the adhesive mid-thickness for all L_O

values. As shown in Figure 59, representing σ_y stresses at the planes of Figure 58, σ_y stresses peak at the overlap edges for all considered planes. This effect is related with the adherends rotation [65] which causes the separation of the edges and therefore compresses the interior zone of the overlap. Actually, at the inner region of the overlap, σ_y stresses are compressive and smaller in magnitude. The σ_y peak stresses at the overlap edges cause a decrease of the joint strength that can lead to premature failures [61, 66]. Typically, σ_y stresses are much smaller in magnitude than τ_{xy} stresses except at the bond edges, in which τ_{xy} stress singularities build up owing to the square-edge geometry [67, 68]. In the composite (planes P1 and P2), σ_y stresses are only important near the stress singularities (x/L_O=0 and x/L_O=1) and quickly vanish within the composite. Due to the different stiffness, the aluminium adherend suffers higher transverse plastic deformation, consequently causing higher σ_y stresses at x/L_O=1. σ_y stresses are mostly smaller than τ_{avg} for all L_O values, except at the overlap edges and are negative in the central part, to ensure equilibrium.

Between all planes, σ_y peak stresses are highest either at plane P3 (x/L_O=0) or at plane P5 (x/L_O=1), i.e., at the stress singularities. This can be explained by the theoretically infinite stresses at these locations. However, the differences between planes are only important at the overlap edges, with minor variations between planes.

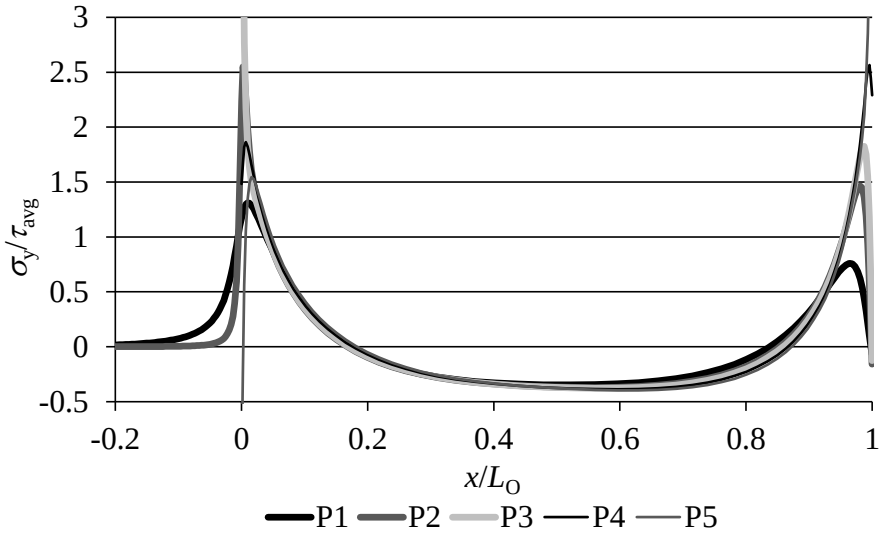

Figure 59 – σ_y stress distributions at the different planes in the joint's height for L_O=10 mm.

σ_y stresses at the adhesive mid-thickness for the different L_O values are presented in Figure 60. σ_y peak stresses increase with L_O, which is known to reduce the joint strength averaged to the bonded area, especially when using brittle adhesives [69]. The ductility of adhesives

partly prevents this limitation of bonded joints because it promotes yielding in the adhesive layer. An increase of the compressive stresses is also found near the singularities with the increase of L_O. Indeed, if σ_y stresses at the ends increase with L_O, the compressive values must also increase in magnitude to enforce equilibrium. These compressive stresses tend to become less significant at the adhesive mid-region. When considering joints between adherends of different stiffness, such as in the present work, different degrees of adherend flexure appear at the overlap edges. Thus, at the rightmost overlap edge, the higher degree of flexure of the more compliant aluminium adherend (compared to the composite) gives σ_y peak stresses with higher magnitude. This should promote damage initiation at this edge rather than at the opposite.

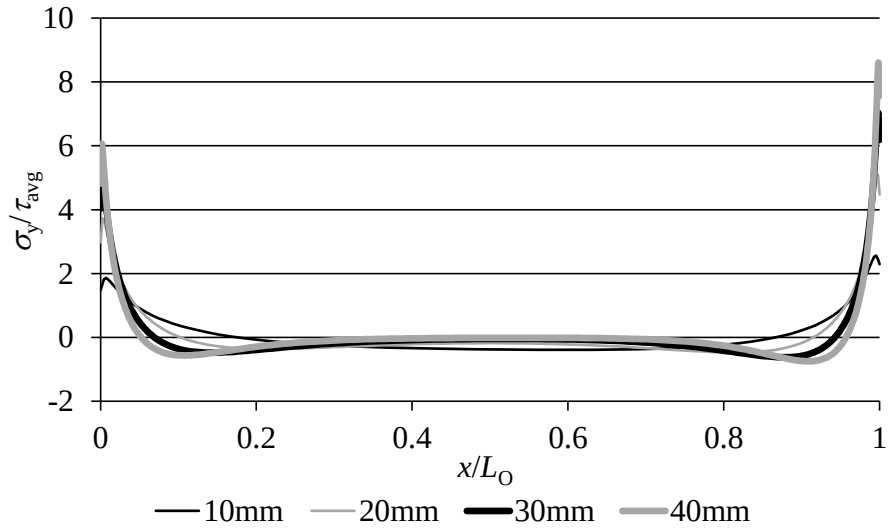

Figure 60 – σ_y stress distributions at the adhesive mid-thickness as a function of L_O

4.3.2 Shear stresses

In this Section, τ_{xy} stress distributions are initially analysed at all different planes for the joint with L_O=10 mm. τ_{xy} stresses for all four L_O values will be then considered as well at the adhesive mid-thickness. The analysis of τ_{xy} stresses at the five planes (Figure 61) shows corresponding results to the σ_y stresses analysed in Section 4.3.1, namely the sites of major stress concentrations, differences between planes and reduced stresses in the composite adherend outside the overlap region. This behaviour is typical for bonded joints [61], and it should be responsible for cohesive failure in the adhesive, provided that the composite through-thickness strength is not smaller than that of the adhesive. The comparative analysis

between planes was extrapolated for all tested L_O values, giving identical results. τ_{xy} stress distributions have the common profiles for this joint configuration, with a progressive increase from the inner part of the overlap to the overlap edges [65, 70, 71]. This occurs due to the different longitudinal deformation of the adherends, as it can be seen in Figure 7. This behaviour is related to the increasing longitudinal straining of the adherends from the free to the opposite overlap edge [72]. At the central area of the overlap, these effects are cancelled, and τ_{xy} stresses are generated solely due to the applied loading. The aluminium experiences higher longitudinal strains than the composite and, due to this difference, τ_{xy} stresses are higher at x/L_O=1 than x/L_O=0.

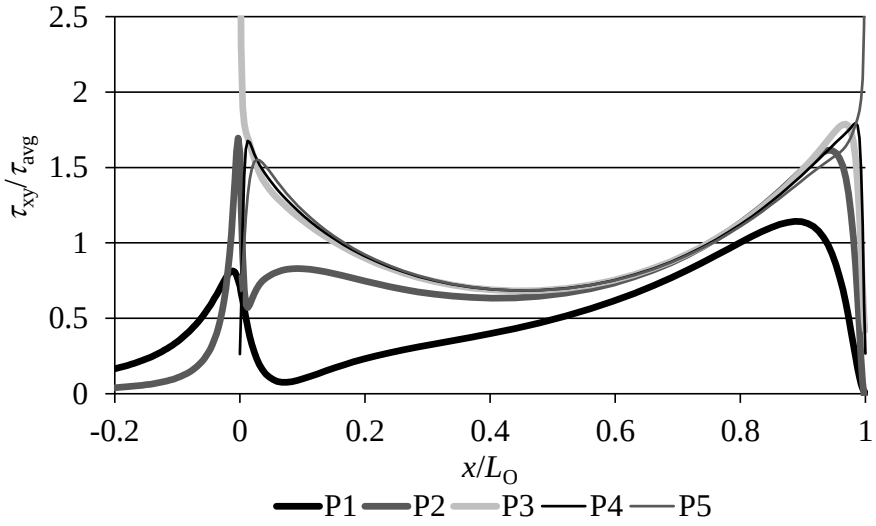

Figure 61 – τ_{xy} stress distributions at the different planes in the joints' height for L_O=10 mm

τ_{xy} stresses at the adhesive mid-thickness for the different L_O values are presented in Figure 62. The reported L_O effect for σ_y stresses, i.e., increase with this parameter, is also found in τ_{xy} stresses. In fact, the increase of L_O promotes higher transmitted loads and differential straining between the adherends, which then reflects on higher τ_{xy} peak stresses [48]. When using brittle adhesives, the overall strength of the joint is affected by the smaller plastic deformation that the adhesive can endure, and the strength improvements with L_O is typically small [50]. In contrast, ductile adhesives allow a better stress distribution in the adhesive mid-region which is put under load gradually when the adhesive at the overlap edges starts to plasticize. This increases the joint strength, which exhibits a significant improvement of P_m with the increase of L_O [61, 73].

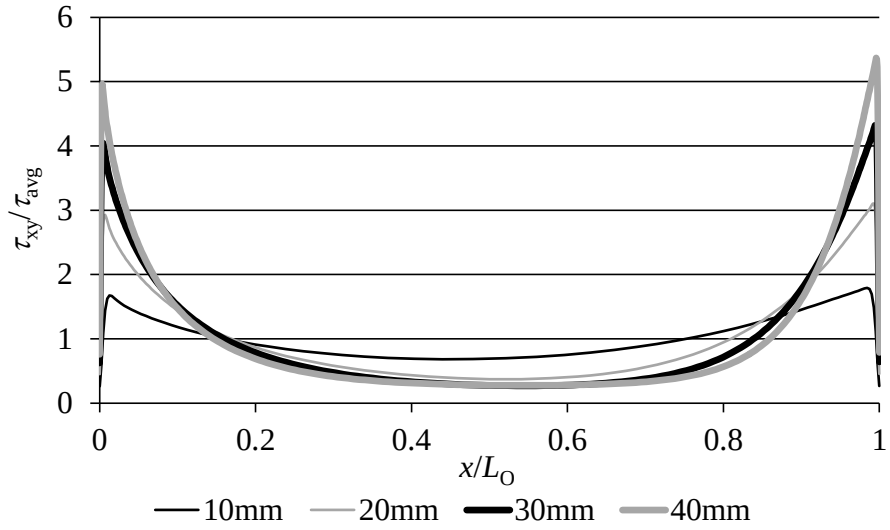

Figure 62 – τ_{xy} stress distributions at the adhesive mid-thickness as a function of L_O

4.4 Damage variable study

The damage variable SDEG of the triangular mixed-mode CZM law (Figure 16) gives the stiffness degradation of the cohesive elements, and it is discussed in this Section for a detailed assessment of the joints' failure. This variable ranges between SDEG=0 (anywhere in the elastic part of the mixed-mode CZM law) and SDEG=1 (failure of the CZM element). All SDEG plots are considered for $0 \leq x/L_O \leq 1$. This damage analysis allows to better understand how damage starts and spreads along the joints and this information will be used in the further discussion regarding the joints' strength.

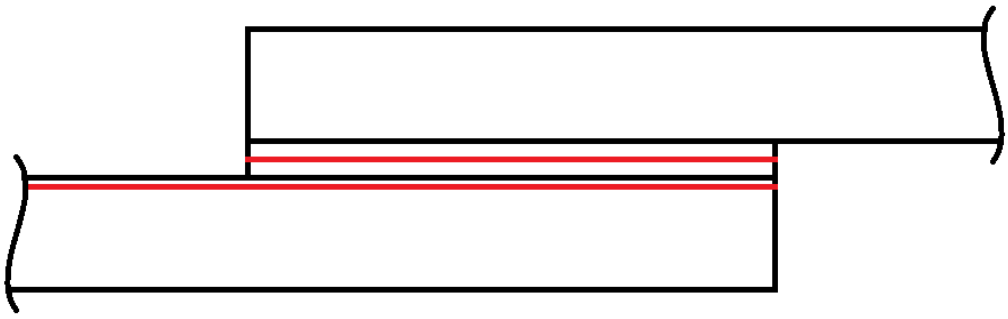

Figure 63 – Horizontal planes considered for the damage analysis

The numerical failure modes are expected to be consistent with the experimental results. Thus, due to the failure paths observed in the experimental work, only two horizontal planes

were considered for the SDEG study, planes P2 and P4. The red lines in Figure 63 represent these planes. Initially, SDEG is plotted at the instant P_m is attained in the joints. The evolution of SDEG with δ is also described for a better perception of the failure process. The presented curves correspond to different values of $\delta/\delta P_m \times 100$ [%] (δP_m is the displacement when P_m is attained).

4.4.1 XNRH6823 damage analysis

Figure 64 shows SDEG for all values of L_O at plane P2 when P_m is reached for the joints bonded with the XNRH6823. In these joints, failure took place very quickly at the most severely stressed plane of the composite (plane P2). This occurs because of the higher mechanical properties of the adhesive, which make the composite to fail prematurely due to the high stresses involved. Analysing Figure 64, it can be found that, at P_m, SDEG peaks at approximately 0.8 for the joint with L_O=10 mm and approximately 0.9 for the remaining joints. The damage starts at x/L_O=1 due to the higher stresses at this location (Figure 60 and Figure 62). The damage progressively decreases towards the inner region of the overlap. With the increase of L_O, damage in the composite at P_m spans to gradually smaller normalized areas, more specifically 54.1% (L_O=10 mm), 11.6% (L_O=20 mm), 7.2% (L_O=30 mm) and 5.7% (L_O=40 mm), which should be related to a small P_m improvement with the increase of L_O.

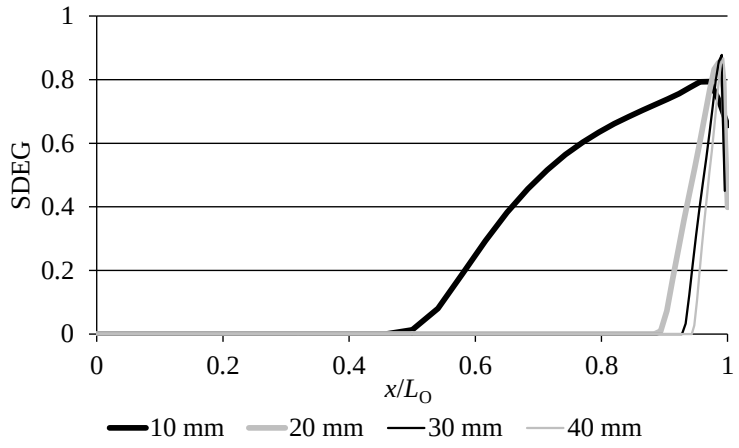

Figure 64 – SDEG across plane P2 at P_m for the joints bonded with the XNRH6823

Figure 65 presents the evolution of SDEG with δ for L_O=10 mm. Failure initiates in the composite at x/L_O=1 and then propagates to the other edge of the overlap. The failure process occurs very swiftly up to x/L_O=0 because of the composite brittleness, resulting in the

transition between no damage to complete failure in a short period of time. Actually, complete failure in the overlap is reached with $\delta/\delta P_m$=100.4%. This reinforces the idea of a diminished improvement of P_m with L_O.

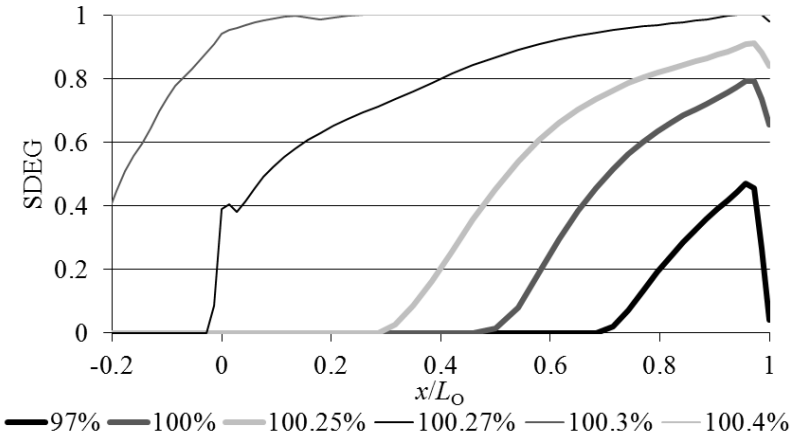

Figure 65 – Evolution of SDEG across the composite (plane P2) with increasing values of $\delta/\delta P_m$ for the hybrid joints bonded with the XNRH6823 and L_O=10 mm

Figure 66 shows an identical analysis but using instead L_O=20 mm. A slight difference regarding the instant when the complete failure is reached. In this case complete failure occurs at $\delta/\delta P_m$=100.52%.

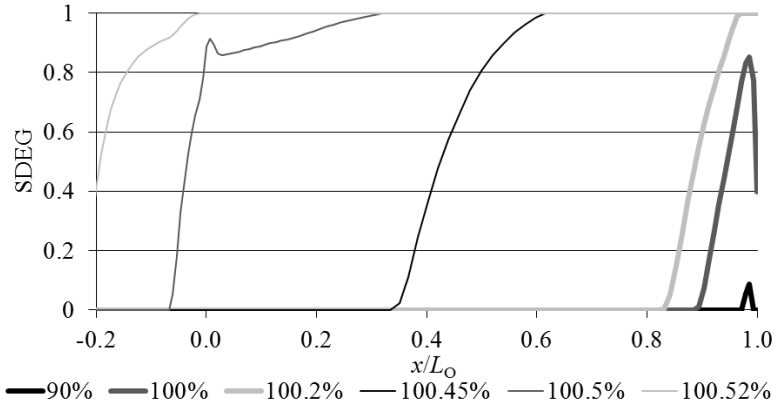

Figure 66 – Evolution of SDEG across the composite (plane P2) with increasing values of $\delta/\delta P_m$ for the hybrid joints bonded with the XNRH6823 and L_O=20 mm

Figure 67 shows the evolution of damage for the joints with L_O=30 mm, and a similar behaviour compared to the joints with L_O=20 mm can be found. Failure occurs at $\delta/\delta P_m$=100.45%.

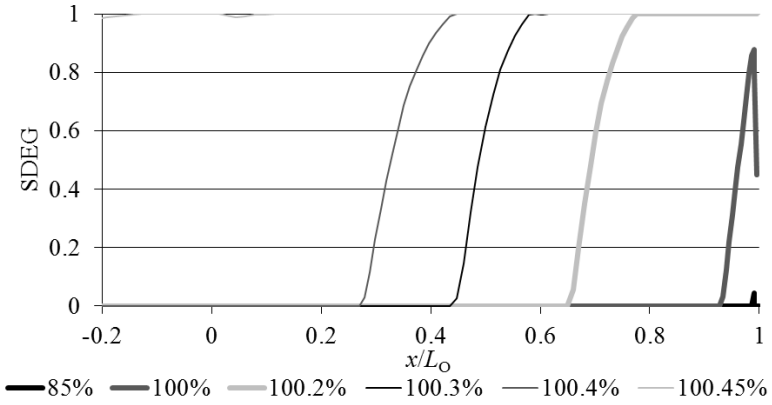

Figure 67 – Evolution of SDEG across the composite (plane P2) with increasing values of $\delta/\delta P_m$ for the hybrid joints bonded with the XNRH6823 and L_O=30 mm

Considering the joint with L_O=40 mm (Figure 68), the overall behaviour is similar. However, P_m occurs with a much more reduced amount of damage in the composite when compared with the other L_O values. Complete overlap failure corresponds to $\delta/\delta P_m$=101%, which is a marginally higher value than for the other L_O values.

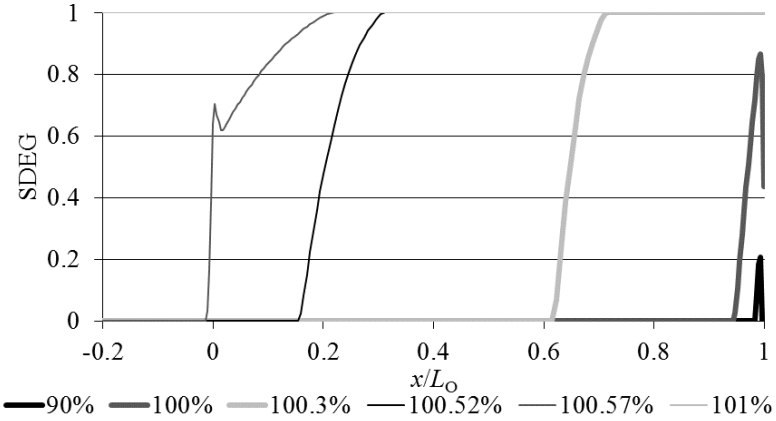

Figure 68 – Evolution of SDEG across the composite (plane P2) with increasing values of $\delta/\delta P_m$ for the hybrid joints bonded with the XNRH6823 and L_O=40 mm

Figure 69 shows SDEG for all values of L_O at plane P4 when P_m is reached for the joints bonded with the XNRH6823. At this plane when P_m is attained the damage is nil for all values of L_O.

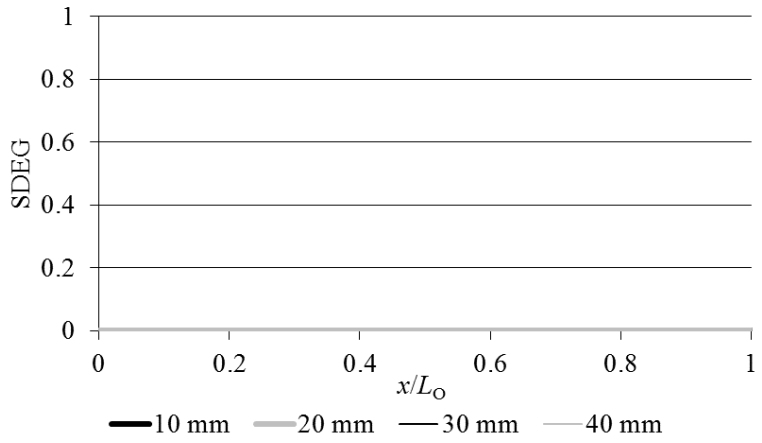

Figure 69 – SDEG across plane P4 at P_m for the joints bonded with the XNRH6823

Analysing the damage evolution at the plane P4 (Figure 70), it can be concluded that the damage in the adhesive is almost nil up to $\delta/\delta P_m$=100.25%. Some degree of damage appears at x/L_O=0, at the opposite overlap edge when compared to the damage in the CFRP, but quickly tends to zero. This is explained by the fact that the composite adherend suffers delamination prior to failure in the adhesive due to the higher mechanical properties of the adhesive. In the joints with L_O=10 mm, at $\delta/\delta P_m$=100.4%, SDEG reaches the maximum value but quickly tends to zero because at this point the CFRP layers fail, as previously discussed.

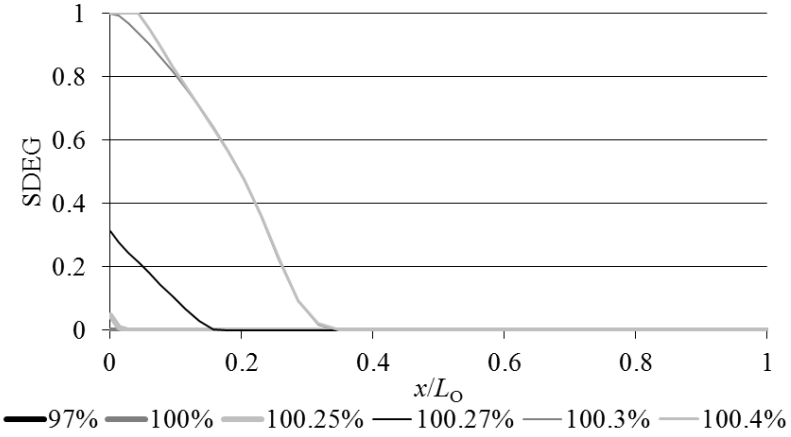

Figure 70 – Evolution of SDEG across the adhesive (plane P4) with increasing values of $\delta/\delta P_m$ for the hybrid joints bonded with the XNRH6823 and L_O=10 mm

The same discussion remains valid for the other three values of L_O. For the joint with L_O=20 mm, the maximum value of SDEG is reached at $\delta/\delta P_m$=100.52%.

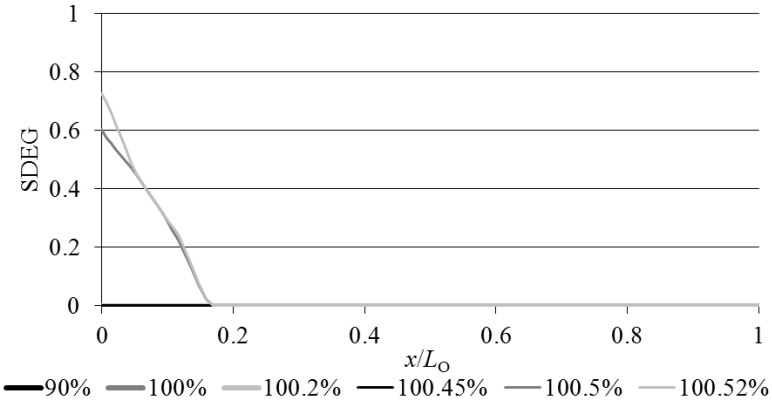

Figure 71 – Evolution of SDEG across the adhesive (plane P4) with increasing values of $\delta/\delta P_m$ for the hybrid joints bonded with the XNRH6823 and L_O=20 mm

For the joint with L_O=30 mm, the maximum SDEG value is reached at $\delta/\delta P_m$=100.45% and quickly tends to zero.

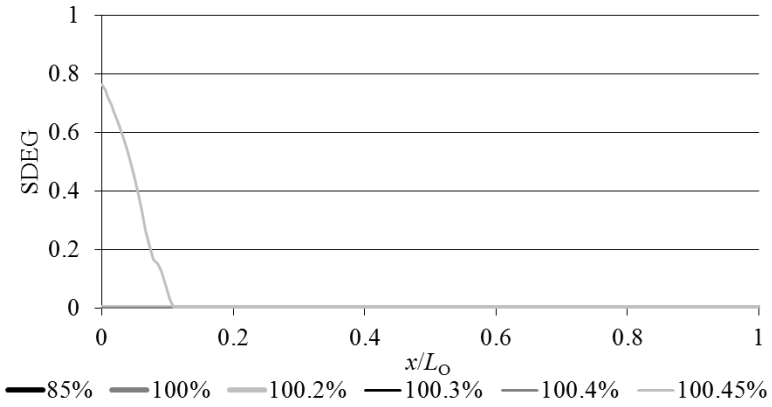

Figure 72 – Evolution of SDEG across the adhesive (plane P4) with increasing values of $\delta/\delta P_m$ for the hybrid joints bonded with the XNRH6823 and L_O=30 mm

For the joint with L_O=40 mm, the maximum value is reached at $\delta/\delta P_m$=101%, in which SDEG reaches 0.8 and then quickly tends to zero.

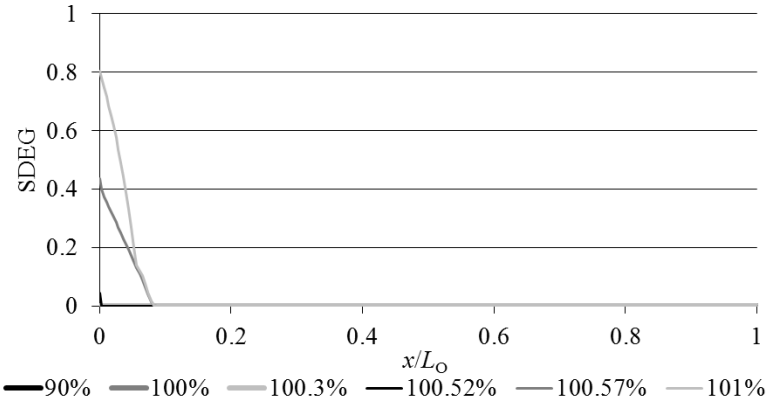

Figure 73 – Evolution of SDEG across the adhesive (plane P4) with increasing values of $\delta/\delta P_m$ for the hybrid joints bonded with the XNRH6823 and L_O=40 mm

4.4.2 XNR6852 damage analysis

The behaviour is markedly different for the joints bonded with the XNR6852, which fail by cohesive failure of the adhesive. Analysing Figure 74, which represents SDEG across the plane P4 when P_m is attained for all L_O values, it is possible to conclude that the damage profile is similar between the different values of L_O.

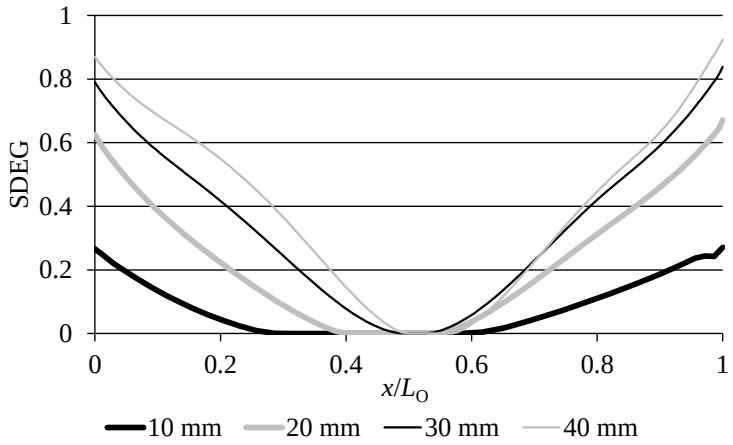

Figure 74 – SDEG across plane P4 at P_m for the joints bonded with the XNR6852

Despite the SDEG plots being unsymmetrical because of the stress distributions' asymmetry (Figure 60 and Figure 62) and different adherends stiffness, the SDEG curves are practically symmetrical with respect to the middle of the adhesive layer. The variation of SDEG through the bondline is much more gradual than for the XNRH6823. The adhesive ductility allows the joint to absorb peak stresses and this smoothens stress distributions. The increase of L_O

is responsible for an increase of overall damage in the adhesive layer at the time of failure. Actually, the percentile portion of the overlap under damage for gradually increasing values of L_O from 10 to 40 mm is 73.7%, 86.3%, 96.0% and 97.3%, by the respective order. This behaviour opposes to the XNRH6823, revealing that the adhesive has a large plasticization ability up to L_O=40 mm, showing that the P_m improvement with this adhesive system should be considerable.

Figure 75 presents the SDEG analysis as a function of δ for the joints bonded with the XNR6852 at plane P4 for L_O=10 mm. Because of the adhesive's ductility and different failure mode, significant discrepancies were found when compared to the joints bonded with the adhesive XNRH6823. Complete failure for the hybrid joint with L_O=10 mm occurs at $\delta/\delta P_m \approx 170\%$, which is a much more gradual failure process than for the XNRH6823, induced by the adhesive ductility (Figure 75).

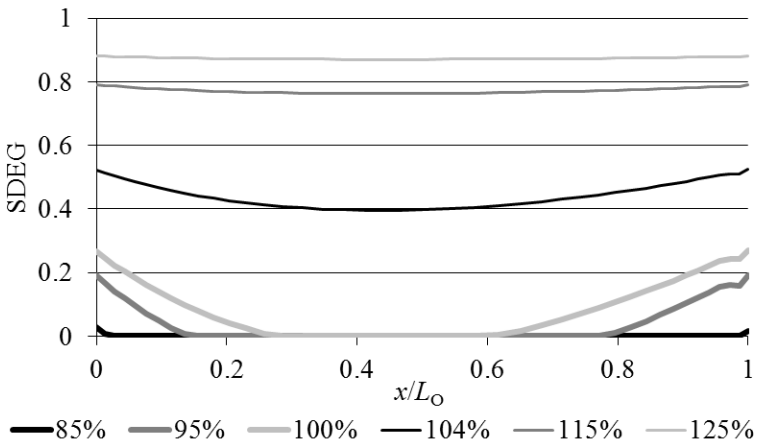

Figure 75 – Evolution of SDEG across the adhesive mid-thickness (plane P4) with increasing values of $\delta/\delta P_m$ for the hybrid joints bonded with the XNR6852 and L_O=10 mm

For L_O=20 mm, $\delta/\delta P_m$ at failure drops to ≈115%, and this is explained by the increase of δP_m with the corresponding increase of L_O. However, the failure process is still gradual when compared with the XNRH6823 (Figure 76).

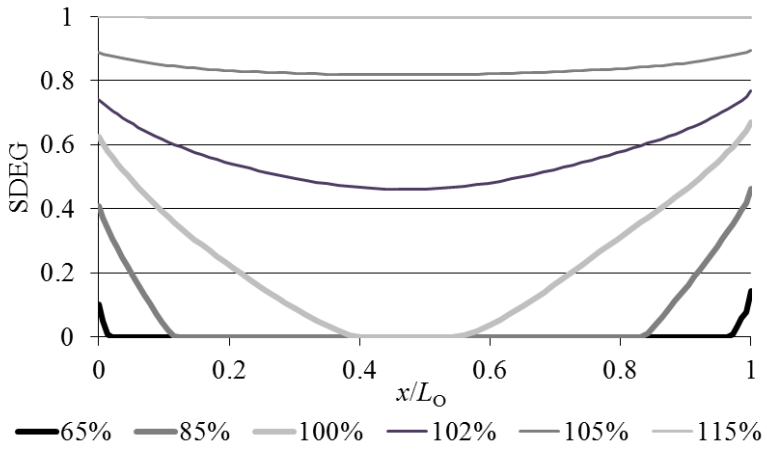

Figure 76 – Evolution of SDEG across the adhesive mid-thickness (plane P4) with increasing values of $\delta/\delta P_m$ for the hybrid joints bonded with the XNR6852 and L_O=20 mm

For L_O=30 mm and L_O=40 mm (Figure 77 and Figure 78, respectively), failure occurs at $\delta/\delta P_m \approx 100.5\%$ and $\delta/\delta P_m \approx 100.22\%$ respectively. This significant reduction of $\delta/\delta P_m$ at joint failure is related to the previously explained reason, i.e., due to the bigger δ value at $\delta/\delta P_m$=100%, induced by the bigger L_O value. The overall behaviour exhibited for the joints bonded with the XNR6852 should be responsible for a significant improvement of P_m with L_O, oppositely to the joints bonded with the XNRH6823.

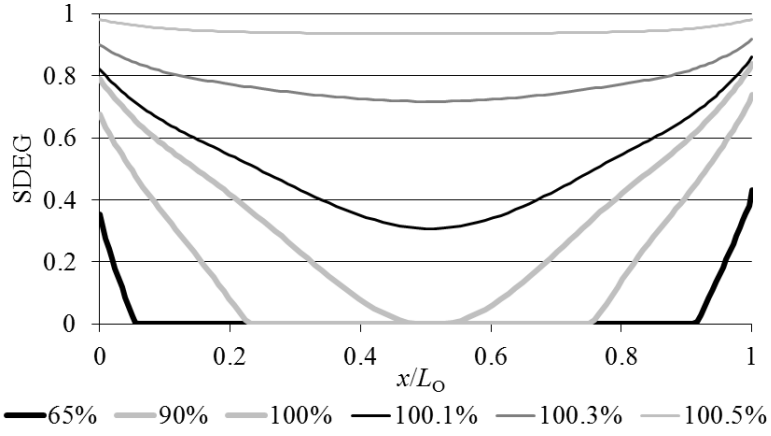

Figure 77 – Evolution of SDEG across the adhesive mid-thickness (plane P4) with increasing values of $\delta/\delta P_m$ for the hybrid joints bonded with the XNR6852 and L_O=30 mm

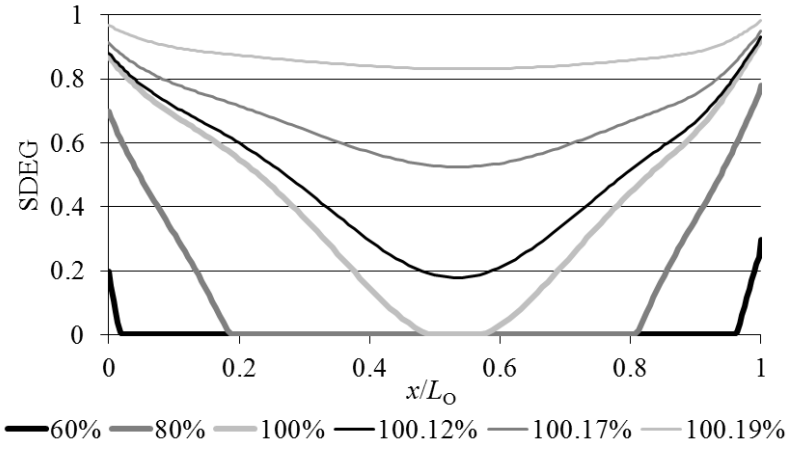

Figure 78 – Evolution of SDEG across the adhesive mid-thickness (plane P4) with increasing values of $\delta/\delta P_m$ for the hybrid joints bonded with the XNR6852 and L_O=40 mm

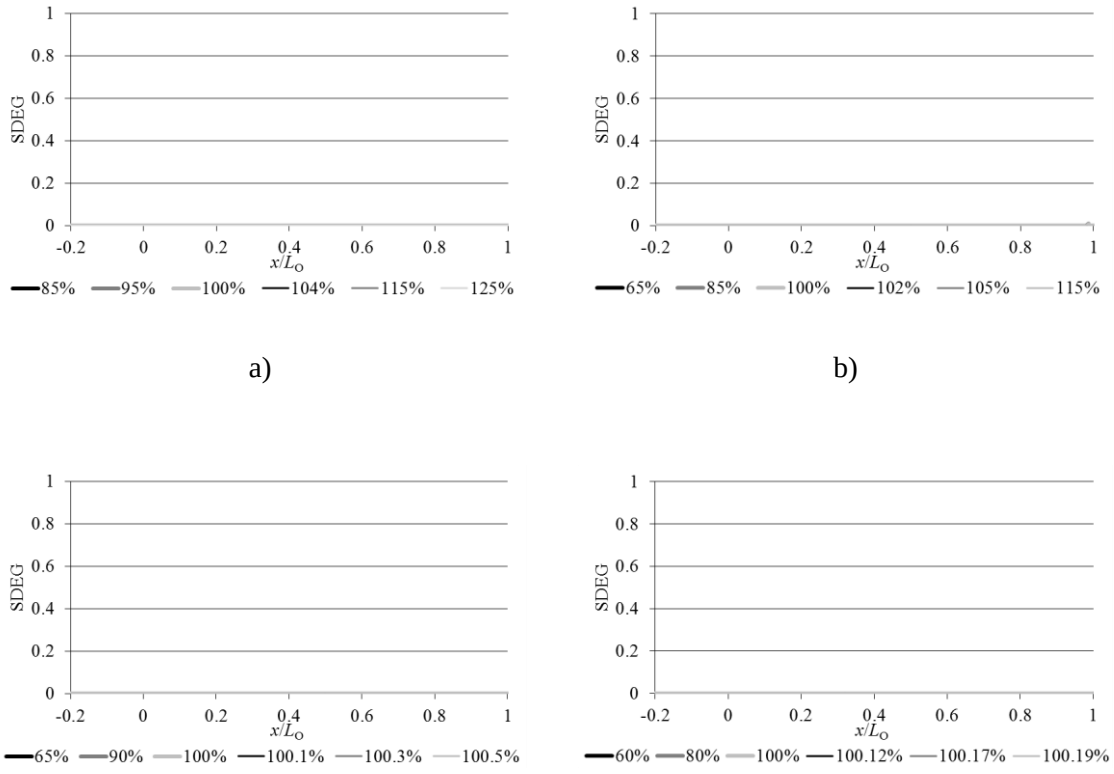

a) b)

c) d)

Figure 79 – Evolution of SDEG across the composite (plane P2) with increasing values of $\delta/\delta P_m$ for the hybrid joints bonded with the XNR6852: L_O=10 mm (a), L_O=20 mm (b), L_O=30 mm (c) and L_O=40 mm (d)

Analysing Figure 79, which represents the damage in the CFRP layers, it is possible to conclude that no damage was found for all values of LO. As explained before, the lower

strength of this adhesive, compared to the XNRH6823, prevents damage in the composite adherend up to complete failure of the joints.

4.5 Failure modes

Likewise in the experimental work, the numerical failure modes were intralaminar for the XNRH6823 and cohesive in the adhesive layer for the XNR6852. Figure 80 and Figure 81 give an example of the numerical failure modes for L_O=10 mm and L_O=40 mm for these adhesives, by the respective order, by showing SDEG after failure. Due to the similarity between the failures modes only two values of L_O are represented.

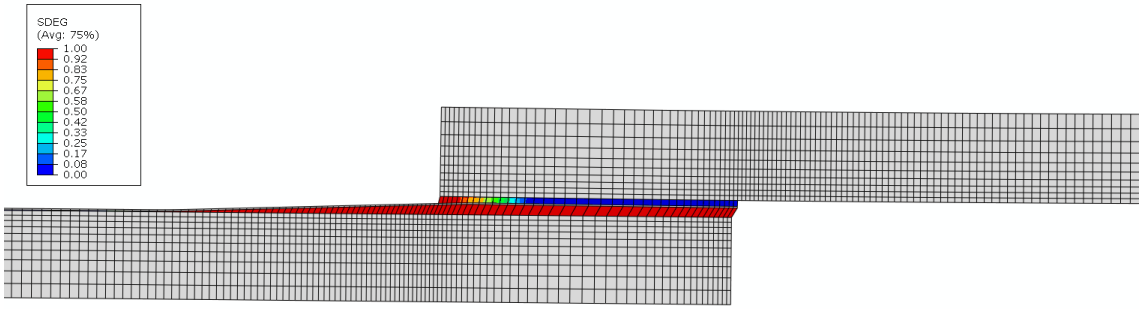

a)

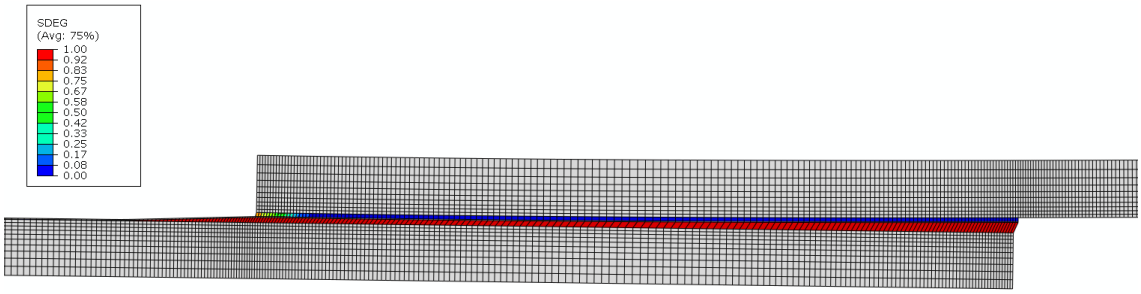

b)

Figure 80 – Intralaminar failure for the joints with XNRH6823: L_O=10 mm (a), L_O=40 mm (b)

The XNRH6823 is stronger and more brittle than the XNR6852, leading to the intralaminar failure of the composite regardless the value of L_O. In this case, the adhesive still exhibited a small amount of damage for L_O=40 mm, but failure occurred through the CFRP. Actually, high stresses are transferred to the CFRP adherends with higher σ_y peel stresses than the

allowable. In this case, damage starts in the composite layers and evolves very quickly because of the brittle fracture of the CFRP. For this reason the increase of L_O does not reflect by a significant amount on P_m. At the edges of the overlap, plastic deformation occurred, although not being significant. This behaviour is consistent with the experimental tests (Figure 45).

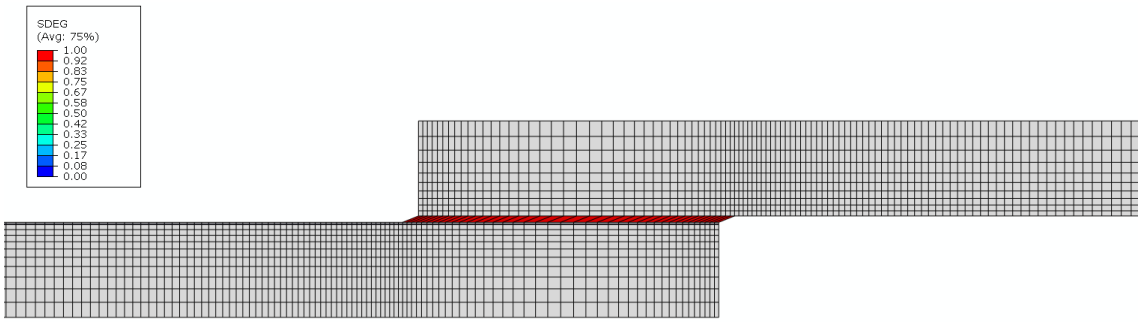

a)

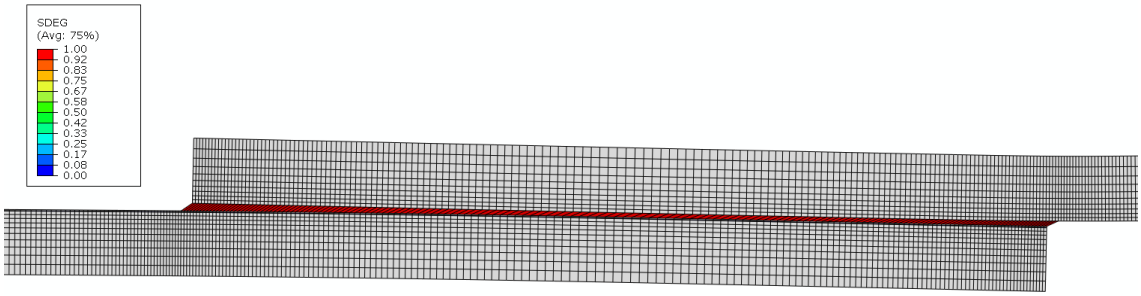

b)

Figure 81 – Cohesive failure of the adhesive for the joints with XNR6852: L_O=10 mm (a), L_O=40 mm (b)

In which regards to the XNR6852, the plastic deformation of the adhesive was higher, as expected by the adhesive properties (Table 11), allowing the joint to sustain higher loads with the increase of the L_O. As it can be found in the damage analyses for the XNR6852, only the adhesive suffered damage, while the CFRP adherend was left intact. Damage started at x/L_O=1 spreading to the inside region. The damage evolution with the applied loading also occurs in a more controlled manner, which explains the improvement of P_m with the increase of the L_O. In the experimental tests it was possible to observe the different colour on the adhesive because of the plastic deformation (Figure 44).

4.6 *P-δ* curves

Figure 82 represent the numerical *P-δ* curves of the joints bonded with the adhesive XNRH6823 for the four different L_O values. As seen in the experimental tests, the curves exhibit a linear behaviour until failure for these bonded joints. The value of P_m is not significantly affected with the increase of L_O.

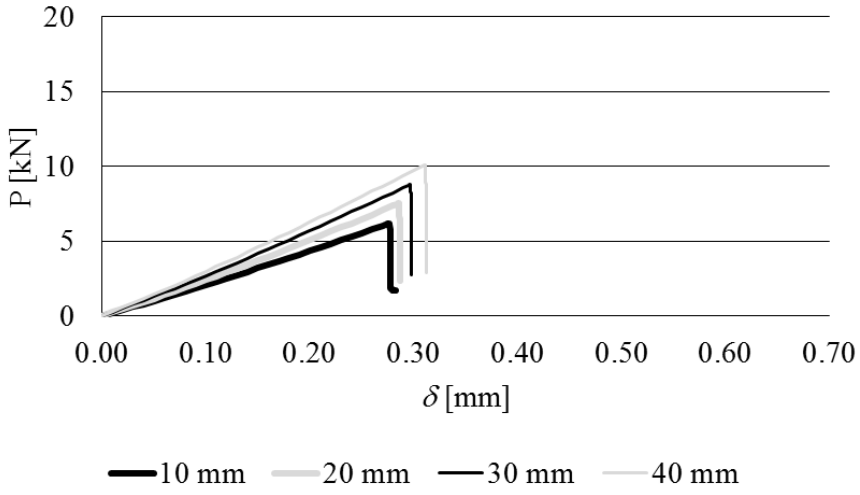

Figure 82 – Numerical *P-δ* curves for the XNRH6823

Analysing Figure 83, the values of P_m of the numerical curves are in close agreement with the experimental ones. In which regards to δP_m, the experimental curves show slightly larger values that increases with the increase of L_O.

Figure 84 represents the numerical *P-δ* curves of the joints bonded with the adhesive XNR6852 for the four different L_O values. Likewise in the joints bonded with the XNRH6823, the numerical curves are very close to the experimental tests but, in contrast, the value of P_m markedly increases with the increase of L_O.

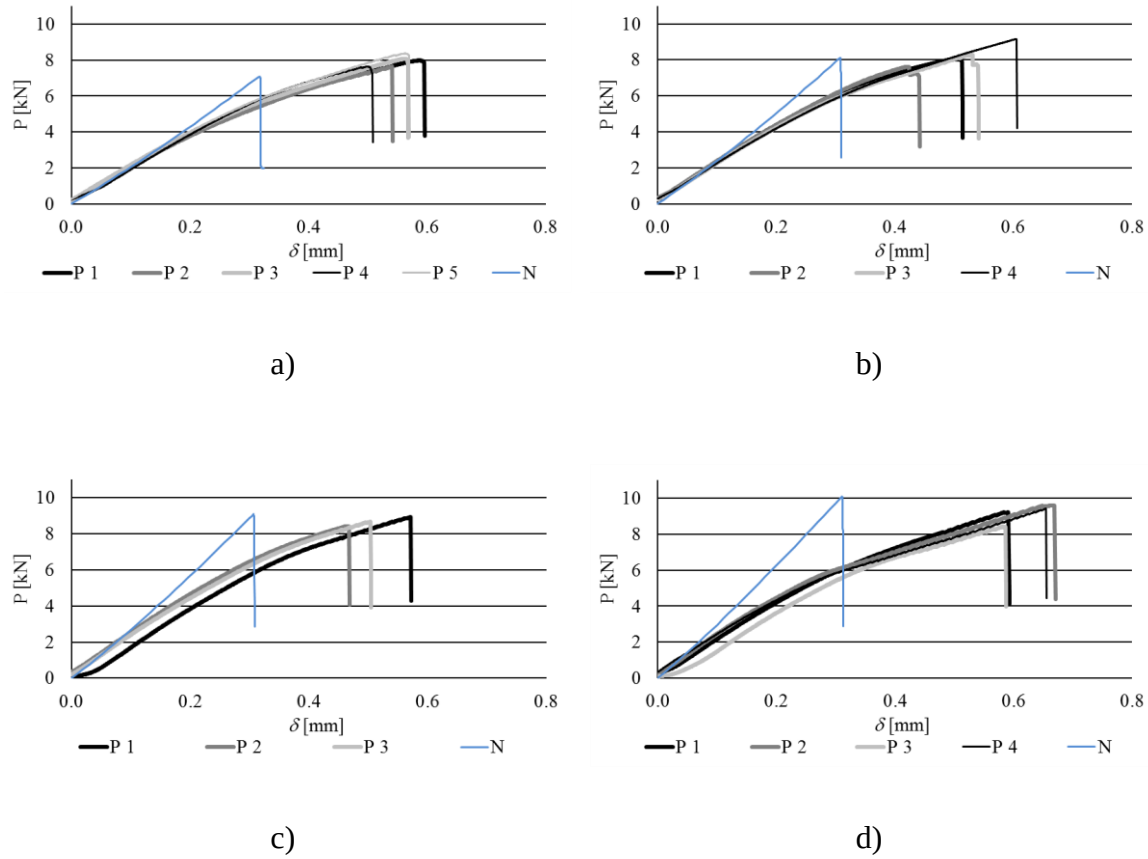

Figure 83 – Comparison between the experimental and numerical *P*-δ curves for the joints bonded with XNRH6823: L_O=10 mm (a), L_O=20 mm (b), L_O=30 mm (c) and L_O=40 mm (d)

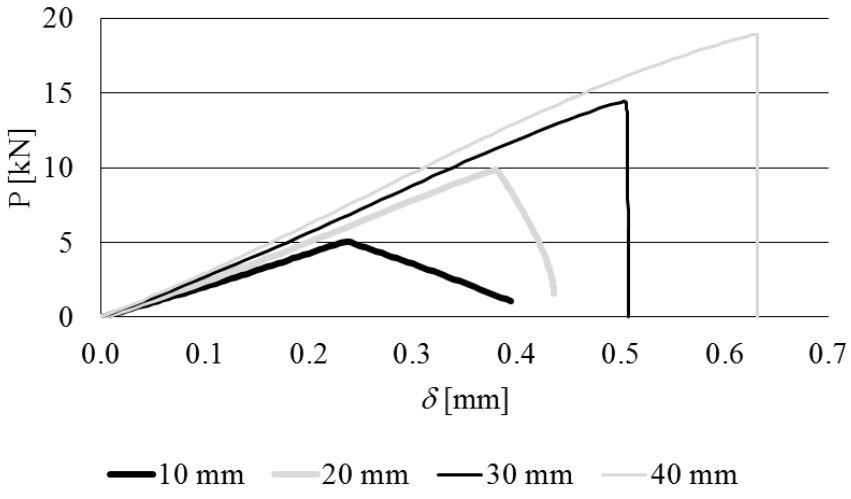

Figure 84 – Numerical *P*-*δ* curves for the XNR6852

Comparing the numerical and the experimental curves of the joints bonded with the adhesive XNR6852 (Figure 85), it can be found that the values of P_m of the numerical curves are in

close agreement with the experimental ones, and the values of δP_m of the experimental curves are slightly higher specially for larger L_O values.

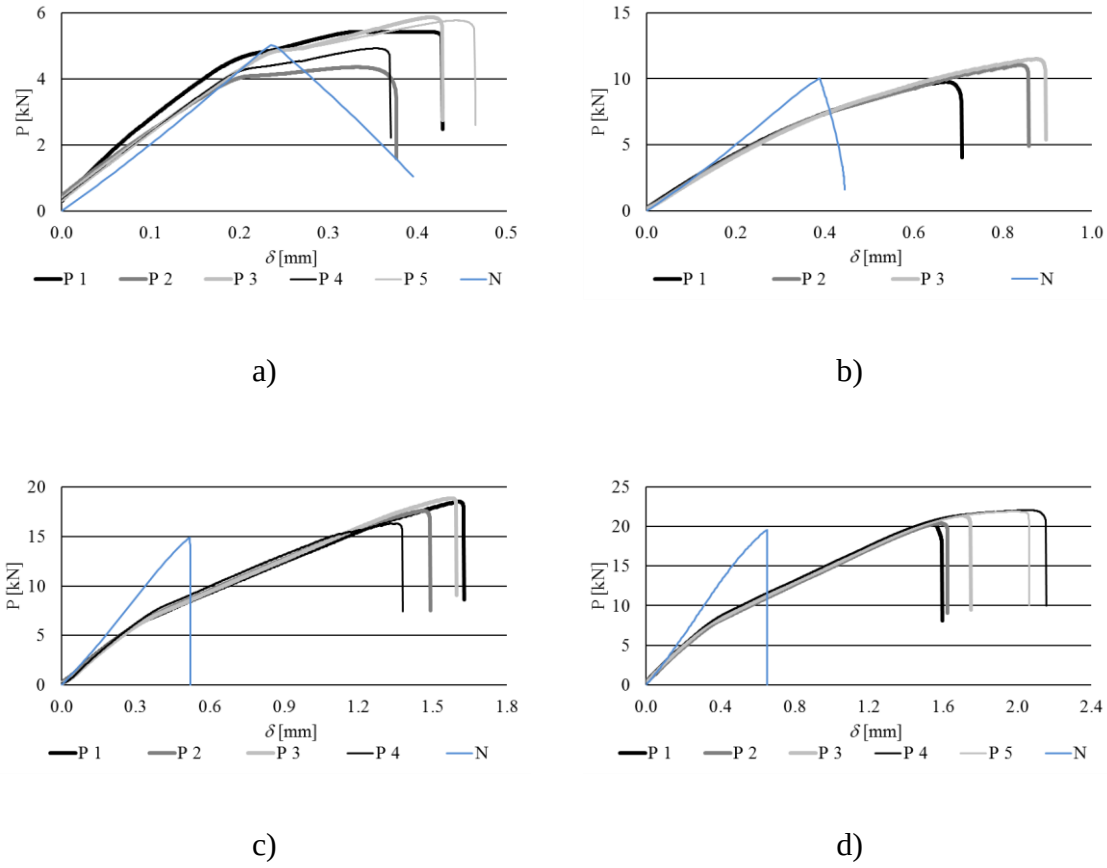

Figure 85 – Comparison between the experimental and numerical *P*-δ curves for the joints bonded with XNR6852: L_O=10 mm (a), L_O=20 mm (b), L_O=30 mm (c) and L_O=40 mm (d)

4.7 Joint strength

Figure 86 and Figure 87 provide the experimental/numerical comparison of P_m vs. L_O for the joints bonded with the XNRH6823 and XNR6852, respectively. The experimental curves represent the average value of the valid specimens for each joint configuration and respective standard deviation.

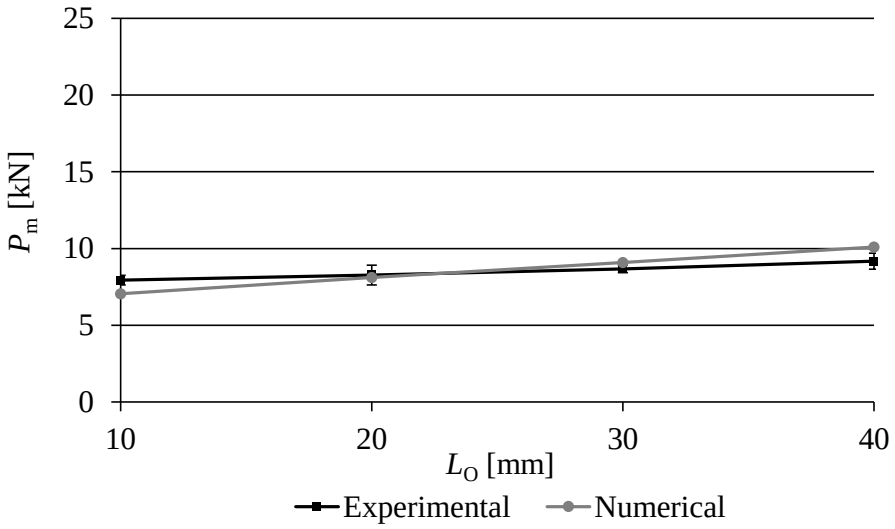

Figure 86 – Experimental and numerical values of P_m vs. L_O for the joints bonded with the adhesive XNRH6823

The results of Figure 86 correspond to a brittle failure in the composite for all joint configurations bonded with the XNRH6823 (Figure 44). Experimental and numerical failures occurred at plane P2 for all joint configurations, and this is related to the significantly smaller peel and shear mechanical properties of the composite compared to those of the adhesive at plane P4 (Table 11), although peak σ_y and τ_{xy} stresses are marginally smaller at plane P2 at x/L_O=1 (Figure 59 and Figure 61) when failure initiates. The brittle failure in the composite for the joints bonded with the XNRH6823 resulted in a very small P_m improvement with L_O, as it can be testified in both experimental and numerical results. Actually, the P_m improvement for L_O=40 mm over L_O=10 mm was 43.4% (numerical) or 15.6% (experimental), which can be compared to the behaviour or bonded joints when brittle failures in the adhesive layer take place [64].

For L_O=10 mm, P_m corresponds to partial degradation of the composite at 54% of L_O, and this damaged length significantly reduces up to L_O=40 mm (damaged portion of L_O was 5.7%). Thus, the composite clearly is not capable of accommodating the peak stresses at the free edge of the adherend, resulting in a brittle failure. The occurrence of a large damage zone for L_O=10 mm, on the other hand, is a result of more uniform stress distributions for short L_O values (Figure 60 and Figure 62) [48]. Figure 68 shows the evolution of SDEG with the applied loading and reinforces this assumption, by testifying the quick failure process up to complete joint failure (values of $\delta/\delta P_m$ at failure of 100.4% for L_O=10 mm and 101% for L_O=40 mm). This behaviour shows a limited benefit in increasing L_O for these joints.

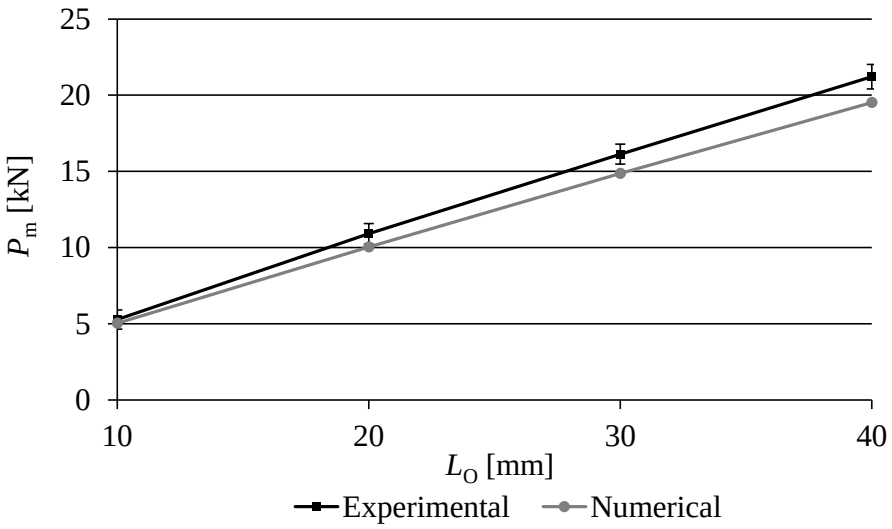

Figure 87 – Experimental and numerical values of P_m vs. L_O for the joints bonded with the adhesive XNR6852

The joints bonded with the XNR6852 showed a linear increase of P_m vs. L_O (Figure 87). As previously mentioned, these joints failed cohesively in the adhesive layer (Figure 45). This can be explained by the inferior adhesive layer strength properties, compared to those of the XNRH6823 (Table 11), promoting premature failure of the adhesive layer with respect to the composite. Although the adhesive's properties are still superior to those of the composite (Table 11), failure in the composite was prevented by overall smaller σ_y and τ_{xy} stresses (Figure 59 and Figure 61), despite at very localised regions this is not exactly true. Both in the experimental and numerical curves the value of P_m always increases up to the biggest value of L_O, which is indicative that the failure strength or at least the yield stress of the CFRP and aluminium adherends was not reached for the obtained P_m values. The stress analysis of Figure 60 (σ_y stresses) and Figure 62 (τ_{xy} stresses) showed that both stress components are more uniform along the bond length for small L_O values. However, since the XNR6852 is highly ductile, it enables plasticization of the adhesive layer beginning at the overlap edges when the limiting stresses are attained, and the joints fail after significant plasticization of the adhesive layer [26]. This justifies the nearly linear evolution of P_m with L_O depicted in Figure 87. Another characteristic of this type of behaviour was the abrupt failure of the specimens, without crack growth before P_m, showing that cracking was prevented at the overlap edges up to P_m being reached [74]. The SDEG analyses also corroborate this assumption. Figure 74 shows that P_m occurs with a significant amount of the adhesive layer under softening (from 73.7% for L_O=10 mm up to 97.3% for L_O=40 mm). Thus, the adhesive layer undergoes extensive plasticization, which reflects on the linear

trend in the P_m vs. L_O plots. The evolution of SDEG with $\delta/\delta P_m$ corroborates this fact (Figure 78), by showing a very gradual evolution of damage and failure under conditions proximal to generalised yielding of the adhesive.

The results of Figure 86 and Figure 87 show that the CZM technique was accurate in predicting the joints' strength for both failure modes, i.e., cohesive failure of the adhesive layer and intralaminar failure of the composite. The maximum deviation between the experiments and numerical simulations for the joints bonded with the XNRH6823, experiencing intralaminar failure in the composite, was 11.2% for L_O=10 mm. The maximum deviation for the joints bonded with the XNR6852, relating to cohesive failure of the adhesive layer, was 8.0% (for L_O=40 mm). In both cases the differences were averaged over the experimental values. The variation observed for the XNRH6823 is justified by inherent issues to composite failures, such as larger properties variations, complexity in the failure modes including fibre bridging events, unstable damage growth, amongst other issues [24]. Nonetheless, the deviation values were quite acceptable. For the XNR6852, the increasing under predictions were clearly caused by the large plastic flow of this adhesive, which is only modelled in an approximated manner by triangular CZM. Despite this fact, the maximum deviation of 8.0% is perfectly acceptable. For more accurate results a trapezoidal cohesive law can be used instead [57].

5 Conclusions

This work aimed at studying, by experimentation and CZM modelling, the tensile behaviour of adhesive single-lap joints between aluminium and CFRP adherends, bonded with a brittle (XNRH6823) and a ductile (XNR6852) adhesive and different L_O values. The main objectives are the analysis of the joints' behaviour and the validation of the numerical tool to predict the joints' strength of joints bonded with the referred adhesives.

After performing the experimental tests, it was concluded that the type of adhesive has a strong impact in the failure modes and P_m. With the adhesive XNRH6823, failure was intralaminar and the increase of L_O had practically no effects in P_m. By contrast, for joints bonded with the adhesive XNR6852, the increase of L_O had a direct effect in P_m such that a nearly increase of P_m with L_O was found. Comparing the two adhesives, the XNRH6823 presented a slightly higher P_m than the XNR6852 for L_O=10 mm but, for increasing L_O values, the XNR6852 presented gradually higher P_m values. The higher plasticity of the XNR6852 enabled stress redistribution when limiting stress is attained and, consequently, the increase of L_O had direct impact in P_m.

In order to perform a detailed analysis of the behaviour of the joints, σ_y and τ_{xy} stress distributions were initially studied and analysed at five different planes in the joints' height, including within the composite. The stress analysis showed that σ_y and τ_{xy} stresses peak at the overlap edges, and that these are highest at the adherends/adhesive interfaces. Stresses between different horizontal planes in the joints are similar, except for some variations in the peak values at the overlap edges. σ_y and τ_{xy} stresses are more uniform for short L_O values and tend to increase stress gradients towards the overlap edges with the increase of L_O. The damage analysis enabled a deeper insight of the joints behaviour, showing a brittle composite fracture occurring for the joints with the brittle adhesive, testified by the short damage length and quick failure process. On the other hand, the joints with the ductile adhesive failed cohesively in the adhesive layer under global yielding conditions, which was corroborated

by the large damage length at the instant of P_m. The joints' behaviour as a function of L_O was consistent with these analyses, with the joints bonded with the brittle adhesive giving a negligible strength improvement with L_O. The joints bonded with the ductile adhesive showed a nearly linear P_m improvement with L_O, which agrees with the global yielding conditions at failure previously detected in the damage analysis. The joints' strength and failure modes were highly dependent on the adhesive, and this behaviour was successfully modelled numerically.

Actually, the numerical results are close to the experiments and, therefore, it can be concluded that this numerical tool can be applied in the analysis of this type of joints for design purposes.

The following suggestions are proposed for future works:

- Comparative evolution of CZM modelling with alternative predictive techniques;
- Using an aluminium adherend with higher value of σ_y in the joints bonded with the adhesive XNR6852 to prevent the plasticization of this component;
- Modify the joint geometry to reduce σ_y peak stresses in the joints bonded with the adhesive XNRH6823, to prevent composite failures (e.g. applying filets at the joints' edges);
- Increase of L_O in the joints bonded with the XNR6852 in order to study how the aluminium adherend plasticization influences the joint strength;
- Evaluate a composite with higher interlaminar strength.

References

[1] Airbus, "Airbus Innovative materials," 2015. [Online]. Available: http://www.airbus.com/innovation/proven-concepts/in-design/innovative-materials/. [Acedido em Março 2015].

[2] Alfa Romeo, "Alfa Romeo partners," 2014. [Online]. Available: https://4c.alfaromeo.com/en/partners. [Acedido em Março 2015].

[3] BMW, "Efficiency & dynamics of the BMW i8," 04 2015. [Online]. Available: http://www.bmw.com/com/en/newvehicles/i/i8/2014/showroom/efficiency_dynamics.html. [Acedido em Março 2015].

[4] A. N. S. Nascimento, "Efeito da espessura do adesivo na resistência de juntas de sobreposição simples, na ligação materiais compósitos," Tese de Mestrado, Faculdade de Engenharia da Universidade do Porto, Porto, 2013.

[5] A. Karac, *Testing adhesives and adhesively bonded joints,* Univerzitet U Zenici: Manual técnico, 2013.

[6] R. D. Adams, Adhesive bonding: Science, technology and applications, Bristol: Woodhead Publishing Ltd, 2005.

[7] Y. M. Ji e K. S. Han, "Fracture mechanics approach for failure of adhesive joints in wind turbine blades," *Renewable Energy,* vol. 65, pp. 23-28, 2014.

[8] P. Silva e D. Santos, *Sika, Seminário Juntas Adesivas,* Porto: Instituto Superior de Engenharia do Porto, 2014.

[9] G. Di Bella, G. Galtieri, E. Pollicino e C. Borselino, "Mechanical characterization of adhesive joints with dissimilar substrates for marine applications," *International Journal of Adhesion & Adhesives,* vol. 41, p. 33–40, 2013.

[10] A. L. Loureiro, L. F. M. da Silva, C. Sato e M. A. V. Figueiredo, "Comparison of the mechanical behaviour between stiff and flexible adhesive joints for the automotive industry," *The Journal of Adhesion,* vol. 86, pp. 765-787, 2010.

[11] D. A. Dillard e A. V. Pocius, The mechanics of adhesion, Amsterdan: Elsevier, 2002.

[12] J. Oñoro, "Adesivos - El reto de unir todo con todo," ETSI Industriales, UPM, Espanha.

[13] E. W. Petrie, Handbook of adhesives and sealants, 2nd ed, New York: McGraw-Hill, 2000.

[14] A. M. G. Pinto, "Ligações Adesivas Entre Materiais Poliméricos com e sem Alteração Superficial dos Subtratos," Tese de Doutoramento, Faculdade de Engenharia da Universidade do Porto, Porto, 2007.

[15] A. B. Pereira e A. B. de Morais, "Influência das tensões de Bordo na Resistncia de Juntas Colada de Sobreposição," *Revista Iberoamericana de Ingenieria Mecánica,* vol. 8, pp. 69-79, 2004.

[16] "Materials research," [Online]. Available: http://www.scielo.br/scielo.php?script=sci_arttext&pid=S1516-1392012000300015. [Acedido em Abril 2015].

[17] L. F. M. da Silva, A. G. de Magalhães e M. F. S. F. de Moura, Juntas Adesivas Estruturais, Porto: Publindústria, 2007, p. 130.

[18] J. H. Kweon, J. W. Jung, T. H. Kim, J. H. Choi e D. H. Kim, "Failure of carbon composite-to-aluminum joints with combined mechanical fastening and adhesive bonding," *International Journal of Adhesion & Adhesives,* vol. 75, pp. 192-198, 2006.

[19] L. M. B. S. Teixeira, "Caracterização do comportamento mecânico de juntas de sobreposição simples coladas com adesivos estruturais," Tese de Mestrado, Faculdade de Engenharia da Universidade do Porto, Porto, 2000.

[20] G. Fessel, J. G. Broughton, N. A. Fellows, J. F. Durodola e A. R. Hutchinson, "Evaluation of different lap-shear joint geometries for automotive applications," *International Journal of Adhesion & Adhesives,* pp. 574-583, 2007.

[21] P. N. B. Reis, J. A. M. Ferreira e F. Antunes, "Effect of adherend's rigidity on the shear strength of single lap adhesive joints," *International Journal of Adhesion & Adhesives,* pp. 193-201, 2011.

[22] D. J. Dunn, Engineering and Structural Adhesives, Akron: iSmithers Rapra Publishing, 2004.

[23] M. S. Seong, T. H. Kim, K. H. Nguyen, J. H. Kweon e J. H. Choi, "A parametric study on the failure of bonded single-lap joints of carbon composite and aluminum," *International Journal of Adhesion & Adhesives,* vol. 86, pp. 135-145, 2008.

[24] T. Kim, J. Kweon e J. Choi, "An experimental study on the effect of overlap length on the failure of composite-to-aluminum single-lap bonded joints," *Journal of Reinforced Plastics and Composites,* pp. 1071-1081, 2008.

[25] B. A. Huppe, "High reliability adhesive joining of metal and composite components," Technology Laboratory for Advanced Composites, Department of Aeronautics and Astronautics, Massachusetts, 2001.

[26] R. D. Adams, J. Comyn e W. C. Wake, Structural adhesive joints in engineering, 2nd ed, London: Chapman & Hall, 1997.

[27] X. Zhao, R. D. Adams e L. F. M. da Silva, "Single lap joints with rounded adherend corners: Experimental results and strength prediction," *Journal of Adhesion Science and Technology,* vol. 25, pp. 837-856, 2011.

[28] R. D. Adams e J. A. Harris, "The influence of local geometry on the strength of adhesive joints.," *International Journal of Adhesion & Adhesives,* vol. 7, pp. 69-80, 1987.

[29] K. Kegami, T. Takeshita, K. Matsuo e T. Sugibayashi, "Strength of adhesively bonded scarf joints between glass fibre-reinforced plastics and metal.," *International Journal of adhesives and adhesion,* vol. 10, pp. 199-206, 1990.

[30] L. F. M. da Silva, R. J. C. Carbas, G. W. Critchlow, M. A. V. Figueiredo e K. Brown, "Effect of material, geometry, surface treatment and environment on the shear strength of single lap joints.," *International Journal of Adhesion & Adhesives,* vol. 29, pp. 621-632, 2009.

[31] J. D. Clarke e I. J. McGregor, "Ultimate tensile stress over a zone: a new failure criterion for adhesive joints," *The Journal of Adhesion,* vol. 42, pp. 227-245, 1993.

[32] M. L. Williams, "The stresses around a fault or crack in dissimilar media," *Bulletin of the Seismic Society of America,* vol. 49, pp. 199-204, 1959.

[33] G. Fernlund e J. K. Spelt, "J-integration with the mode partition," *International Journal of Adhesion & Adhesives,* 1991.

[34] D. A. Dillard, Advances in structural adhesive bonding, Sawston: Woodhead Publishing, 2010.

[35] H. L. Groth, "Stress singularities and fracture at interface corners in bonded joints," *International Journal of Adhesion & Adhesives,* vol. 8, pp. 107-113, 1988.

[36] D. M. Gleich, M. J. L. van Tooren e A. Beukers, "Analysis and evaluation of bond line thickness effects on failure load in adhesively bonded structures," *Journal of Adhesion Science and Technology,* vol. 15, pp. 1091-1101, 2001.

[37] J. R. Rice, "A path independent integral and the approximate analysis of strain concentration by notches and cracks," *Journal of Applied Mechanics,* vol. 35, pp. 379-386, 1968.

[38] D. S. Dugdale, Yielding of steel sheets containing slits, Chicago: Elsevier, 1960.

[39] G. I. Barenblatt, "The formation of equilibrium cracks during brittle fracture," *Journal of Applied Mathematics and Mechanics,* vol. 23, p. 622–636, 1959.

[40] P. Feraren e H. M. Jensen, "Cohesive zone modelling of interface fracture near flaws in adhesive joints," *Engineering Fracture Mechanics,* vol. 71, p. 2125–2142, 2004.

[41] M. J. Lee, "Determination of cohesive parameters for a mixed-mode cohesive zone model," *International Journal of Adhesion & Adhesives,* vol. 30, pp. 322-328, 2010.

[42] T. Pardoen, T. Ferracin, C. M. Landis e F. Delannay, "Constraint effects in adhesive joint fracture," *Journal of the Mechanics and Physics of Solids,* vol. 53, p. 1951–1983, 2005.

[43] D. Xie e A. M. Waas, "Discrete cohesive zone model for mixed-mode fracture using finite element analysis," *Engineering Fracture Mechanics,* vol. 73, p. 1783–1796, 2006.

[44] R. D. S. G. Campilho, A. M. G. Pinto, M. D. Banea e L. F. M. da Silva, "Optimization study of hybrid spot-welded/bonded single-lap joints," *International Journal of Adhesion & Adhesives,* vol. 37, pp. 86-95, 2012.

[45] Q. D. Yang e M. D. Thouless, "Mixed-mode fracture analyses of plastically-deforming adhesive joints.," *International Journal of Fracture,* vol. 110, pp. 175-187, 2001.

[46] L. F. M. da Silva e R. D. S. G. Campilho, Advances in Numerical Modelling of Adhesive Joints, Berlin: Springer, 2012.

[47] L. D. Jofre e E. O. Julián, "Durability of Adhesively-Bonded CFRP/Steel Joints," Tese de Mestrado, Chalmers University of Technology, Göteborg, 2013.

[48] R. D. S. G. Campilho, M. D. Banea, A. M. G. Pinto, L. F. M. da Silva e A. M. P. de Jesus, "Strength prediction of single and double-lap joints by standard and extended finite element modeling," *International Journal of Adhesion & Adhesives,* vol. 31, p. 363–372, 15 02 2011.

[49] "Aalco Metals Limited," 2015. [Online]. Available: http://www.aalco.co.uk/datasheets/Aluminium-Alloy-6082-T6T651-Plate_148.ashx. [Acedido em Maio 2015].

[50] T. A. B. Fernandes, "Aplicação de métodos numéricos avançados para a previsão de resistência de ligações adesivas," Tese de Mestrado, Instituto Superior de Engenharia do Porto, Porto, 2014.

[51] R. M. Guedes, M. A. Vaz, F. J. Ferreira e J. L. Morais, "Response of CFRP Laminates under High Strain Rate Compression until Failure," *Science and Engineering of Composite Materials,* vol. 12, 2005.

[52] R. D. S. G. Campilho, "Repair of composite and wood structures," Tese de Doutoramento, Faculdade de Engenharia da Universidade do Porto, Porto, 2009.

[53] Nagase ChemteX Corporation, *Technical information sheet XN6823LM,* 2011.

[54] Nagase ChemteX Corporation, *Tecnhical information sheet XNR6852,* 2012.

[55] Dremel. [Online]. Available: http://www.rccaraction.com/wp-content/uploads/2013/08/dremelcover.jpg. [Acedido em Abril 2015].

[56] R. D. S. G. Campilho, M. F. S. F. d. Moura e J. J. M. S. Domingues, "Using a cohesive damage model to predict the tensile behaviour of CFRP single-strap repairs," *International Journal of Solids and Structures,* pp. 1497-1512, 2008.

[57] R. D. S. G. Campilho, M. D. Banea, J. A. B. P. Neto e L. F. M. da Silva, "Modelling adhesive joints with cohesive zone models: effect of the cohesive law shape of the adhesive layer," *International Journal of Adhesion & Adhesives,* vol. 44, pp. 48-56, 2013.

[58] C. D. M. Liljedahl, A. D. Crocombe, M. A. Wahab e I. A. Ashcroft, "Damage modelling of adhesively bonded joints," *International Journal of Fracture,* vol. 141, pp. 147-161, 2006.

[59] R. D. S. G. Campilho, M. F. S. F. de Moura, A. M. G. Pinto, J. J. L. Morais e J. J. M. S. Domingues, "Modelling the tensile fracture behaviour of CFRP scarf repairs," *Composites Part B: Engineering,* pp. 149-157, 2009.

[60] Dassault Systèmes, *Abaqus Documentation.,* Vélizy-Villacoublay, 2009.

[61] R. D. S. G. Campilho, M. F. S. F. de Moura e J. J. M. S. Domingues, "Modelling single and double-lap repairs on composite materials," *Composites Science and Technology,* pp. 1948-1958, 2005.

[62] A. B. Pereira e A. B. de Morais, "Strength of adhesively bonded stainless steel joints," *International Journal of Adhesion & Adhesives,* pp. 315-322, 2003.

[63] G. Ji, Z. Ouyang, G. Li, S. Ibekwe e S. S. Pang, "Effects of adhesive thickness on global and local Mode-I interfacial fracture of bonded joints.," *International Journal of Solids and Structures,* vol. 47, pp. 2445-2458, 2010.

[64] J. A. B. P. Neto, R. D. S. G. Campilho e L. F. M. da Silva, "Parametric study of adhesive joints with composites," *International Journal of Adhesion & Adhesives,* vol. 37, pp. 96-101, 2012.

[65] B. Zhao, Lu, Z. H. e Y. N. Lu, "Two-dimensional analytical solution of elastic stresses for balanced single-lap joints – Variational method," *International Journal of Adhesion & Adhesives,* vol. 49, pp. 115-126, 2014.

[66] R. D. S. G. Campilho, M. F. S. F. de Moura e J. J. M. S. Domingues, "Numerical prediction on the tensile residual strength of repaired CFRP under different geometric changes," *International Journal of Adhesion & Adhesives,* vol. 29, pp. 195-205, 2009.

[67] J. Radice e J. Vinson, "On the use of quasi-dynamic modeling for composite material structures: analysis of adhesively bonded joints with midplane asymmetry and transverse shear deformation," *Composites Science and Technology,* vol. 66, pp. 2528-2547, 2006.

[68] A. A. Taib, R. Boukhili, S. Achiou e H. Boukehili, "Bonded joints with composite adherends. Part I. Effect of specimen configuration, adhesive thickness, spew fillet and adherend stiffness on fracture," *International Journal of Adhesion & Adhesives,* pp. 237-248, 2006.

[69] P. Reis, F. Antunes e J. A. M. Ferreira, "Influence of superposition length on mechanical resistance of single lap adhesive joints.," *Composite Structures,* vol. 67, pp. 125-133, 2005.

[70] M. Vable e J. R. Maddi, "Boundary element analysis of adhesively bonded joints," *International Journal of Adhesion & Adhesives,* vol. 26, pp. 133-144, 2006.

[71] Q. Luo e L. Tong, "Fully-coupled nonlinear analysis of single lap adhesive joints," *International Journal of Solids and Structures,* vol. 44, pp. 2349-2370, 2007.

[72] W. Jiang e P. Qiao, "An improved four-parameter model with consideration of Poisson's effect on stress analysis of adhesive joints," *Engineering Structures,* vol. 88, pp. 203-215, 2015.

[73] M. Davis e D. Bond, "Principles and practices of adhesive bonded structural joints and repairs," *International Journal of Adhesion & Adhesives,* vol. 19, pp. 91-105, 1999.

[74] F. Z. Hu e C. Soutis, "Strength prediction of patch repaired CFRP laminates loaded in compression.," *Composites Science and Technology,* vol. 60, pp. 1103-1114, 2000.